UNIVERSITY OF TARTU
Institute of Computer Science
Computer Science Curriculum

Alessandro Stranieri

Analysis of the aperiodic component in the mouse neocortex

Master's Thesis (30 ECTS)

Supervisor: Jaan Aru, PhD

Tartu 2021

Analysis of the aperiodic component in the mouse neocortex

Abstract:
Neuronal activity that underlies the conscious and unconscious aspects of animal life can manifest and be measured in different ways. The understanding of what is happening in the brain is a paramount objective of neuroscience. With the increasing availability of data and better analysis tools, we are seeing this objective becoming closer to our reach.

The electrical activity recorded from the brain can display oscillations at specific frequencies in conjunction with physiological or behavioral states. These periodic components have been associated to animal (including human) behavior and even used to diagnose physiological abnormalities. In more recent years, the notion that only periodic components provide a view into brain activity has been somewhat challenged. Brain signals can also show changes in wider ranges of the spectrum, not linked to any periodic process. This aperiodic component has been already associated to changes in age, but recent studies have begun to show how they could provide a window to more physiological phenomena occurring in the brain.

In this work we investigate how two different types of physiological changes are reflected by changes in the aperiodic component. To that end we analysed data recorded in the primary sensory and motor cortex of mice. To analyze the aperiodic component changes, we used a novel tool that extracts it from a signal, separating it from the periodic components. In our first study, we observed that sensory stimulation correlates with an increase of the aperiodic component in the sensory cortex. In our second analysis we focused on changes occurring under the effect of a receptor blocking drug applied to the primary sensory cortex. Within the area affected by the drug, we observed a decrease in the aperiodic offset and a decrease in correlation of the aperiodic components extracted at different layers. In two out of three mice we also observed this change in the primary motor cortex.

These results help to develop our understanding of the mechanisms underlying the aperiodic contributions to the brain's recorded activity. At the same time, they could potentially enable the use of metrics based on aperiodic activity as a diagnostic tool for mental conditions in health and disease.

Keywords:
Computational Neuroscience; Signal processing;

CERCS: P170 - Computer science, numerical analysis, systems, control; B640 - Neurology, neuropsychology, neurophysiology

Aperioodilise komponendi analüüs hiire ajukoores

Lühikokkuvõte:

Neuraalne aktiivsus, mis on aluseks loomade elu teadlikele ja teadvustamata aspektidele, võib avalduda erinevatel viisidel ning ka selle mõõtmiseks on erinevaid võimalusi. Arusaam ajus toimuvatest protsessidest on neuroteaduse peamine eesmärk. Andmete ja paremate analüüsivahendite kättesaadavuse suurenedes oleme hakanud sellele eesmärgile lähemale jõudma.

Ajus mõõdetud elektrilises aktiivsuses võib teatud sagedustel täheldada võnkeid, mis esinevad koos füsioloogiliste või käitumuslike seisunditega. Neid perioodilisi komponente on seostatud loomade (sh inimeste) käitumisega ja neid on kasutatud isegi füsioloogiliste kõrvalekallete diagnoosimiseks. Viimastel aastatel on mõneti hakatud kahtluse alla seadma väidet, et ainult perioodilised komponendid annavad ülevaate ajutegevusest. Aju signaalid võivad muutuda ka spektri laiemates vahemikes, olemata seotud ühegi perioodilise protsessiga. Seda aperioodilist komponenti on juba seostatud vanuse muutumisega, ent hiljutised uuringud on näidanud, kuidas see võib anda võimaluse uurida ka ajus toimuvaid füsioloogilisi protsesse.

Selles töös uurime, kuidas muutused aperioodilises komponendis tähistavad kaht erinevat tüüpi füsioloogilisi muutusi. Selleks analüüsisime hiirte primaarses sensoorses ja motoorses ajukoores mõõdetud andmeid. Aperioodilise komponendi muutuste analüüsimiseks kasutasime uudset vahendit, mis ekstraheerib selle ajusignaalist, eraldades aperioodilise komponendi perioodilistest komponentidest. Esimeses uuringus täheldasime, et sensoorne stimulatsioon korreleerub aperioodilise komponendi suurenemisega sensoorses ajukoores. Teises analüüsis keskendusime muutustele, mis esinesid retseptorit blokeeriva ravimi toimel, mida rakendati primaarsele sensoorsele ajukoorele. Ravimiga töödeldud piirkonnas täheldasime aperioodilise nihke vähenemist ja erinevatest kihtidest ekstraheeritud aperioodiliste komponentide korrelatsiooni vähenemist. Kahe hiire puhul mõõtsime sarnaseid muutuseid ka esmases motoorses korteksis.

Need tulemused aitavad arendada meie arusaama mehhanismidest, mis on ajuaktiivsuse aperioodilise komponendi aluseks. Samuti võivad need potentsiaalselt võimaldada aperioodilisel aktiivsusel põhinevate mõõdikute kasutamist vaimsete häirete ning füsioloogiliste protsesside diagnostikas.

Võtmesõnad:
Arvutuslik neuroteadus; Signaalitöötlus;

CERCS:P170 - Arvutiteadus, arvutusmeetodid, süsteemid, juhtimine (automaatjuhtimisteooria); B640 - Neuroloogia, neuropsühholoogia, neurofüsioloogia

Acknowledgements

First of all, I would like to thank my supervisor Jaan Aru. You have given me the chance to work on this vast and very complicated field, and I am honored that I was able to work with you. Through your comments and patient suggestions, I have learned so much.

I would also like to thank Mototaka Suzuki for making available the data used in this study.

This has been quite the ride, and it would not have been possible without two very important persons that have always given me unconditional support.

Dear Inga, what a year we have had. And I am not referring to the pandemic! This is not the time and place to list all the things and troubles we went through but, it seems we are finally seeing the coming of some brighter days. I personally would have not made it sanely completing this work without you by my side. I had this crazy idea, and you were there for me. You are truly my *elukaaslane*, my life-partner.

My most sincere gratitude goes also to my sister Angelica: the real scientist. You have encouraged me all along, put a straight face whenever I uttered my usual nonsense and listened to my daily frustration reports. Thanks to you, I also realized that it is OK to be inspired by someone younger than yourself.

Contents

1 Introduction

1.1 Listening to the brain

In the quest to understand how the brain works, there are several questions that one might pose. How does the brain produce behaviour? What are the elements involved in creating the mind? What are the mechanisms through which these elements interact and from which the mind emerges? In this work, we obviously do not intend to undertake the task of answering any of these questions, but we believe it is important to hold in mind the motivation behind our work. Our more concrete goal here is to uncover measurable relationships between physiological phenomena occurring in the brain and its electrical activity.

The brain is the host of a large amount of concurrent activities. Neurons are firing at different intervals and intensities; blood flows across different regions; connections among neurons are created, strengthened or weakened. We are already capable of observing and recording a great deal of the phenomena that take place, but the challenge of decoding them and understand them is still open and active [CS15].

There are several techniques and technologies that are used to study the brain in action. Single ion channels can be observed with X-ray crystallography [Kre07]. Single-neuron signal resolution is allowed by micro-electrodes planted near a neuron's cell body, allowing to record sequences of its action potentials (also known as spikes). With arrays of micro-electrodes implanted in specific regions of the cortex it is possible to record Local Field Potential (LFP) of an ensemble of neurons. LFP recordings can account for neuronal activity within 250 μm from the recording site [KNB$^+$09] and have been extensively used in experiments focused on sensory, motor and cognitive functions. In Electroencephalography (EEG) the voltage fluctuations generated by neuronal activity are recorded by electrodes placed on the scalp. Electrocorticography (ECoG) is a more invasive technique, in which the electrodes are placed directly on the surface of the brain. Magnetoencephalography (MEG) devices record neuronal activity by exploiting the magnetic fields created by the electrical currents resulting by neuronal activity. Calcium signaling is the change in concentration of Ca^{2+} ions across neuronal membranes. This process can reflect synaptic activity and there is a variety of techniques to image these signals in vitro and more recently in vivo [GK12].

In this work, we analyze signals produced by groups of neurons recorded at different depths from the cortex of the mouse brain. We attempt to discover what type of new information these signals might contain and connect it to the brain's physiology. This type of relationships could for example become the basis for diagnostic methods, in which the detection of a feature in the in brain signal helps the classification of physiological states in health and disease.

1.2 Contents

The rest of this manuscript is structured as follows. Section 2 is dedicated to the background of this work. In Section 3, we describe the data and the tools used to perform the analysis of this work. Section 4 contains detailed descriptions of the analyses carried out on the two datasets and the results gathered. In Section 5 we will review the our initial goals in the context of the work done to achieve them. Finally, in Section 6, we summarize the contribution of this work and we will propose new ideas for future investigations.

2 Background

It has been known since early experiments in the 19^{th} century, that brain signals can contain rhythmic patterns [Ber29]. That is, creating a representation of the signal in the frequency domain would reveal the presence of oscillatory components at specific frequency bands. These components can be found over a very large range of frequencies (1-500 Hz, [Buz04]). In neuroscience works, the definition of these frequency bands can vary slightly. Here we follow this classification: delta (1-4 Hz), theta (4-8 Hz), alpha (8-12 Hz), beta (12-30 Hz), gamma (30-70 Hz), high-gamma (70-150 Hz).

Figure 1a shows a simulation of a brain signal containing two sine-wave functions oscillating at fixed frequencies. A representation of the signal in the frequency domain will show the presence of the two components as peaks (Figure 1b). A band-pass filter can then extract the two components (Figure 1c).

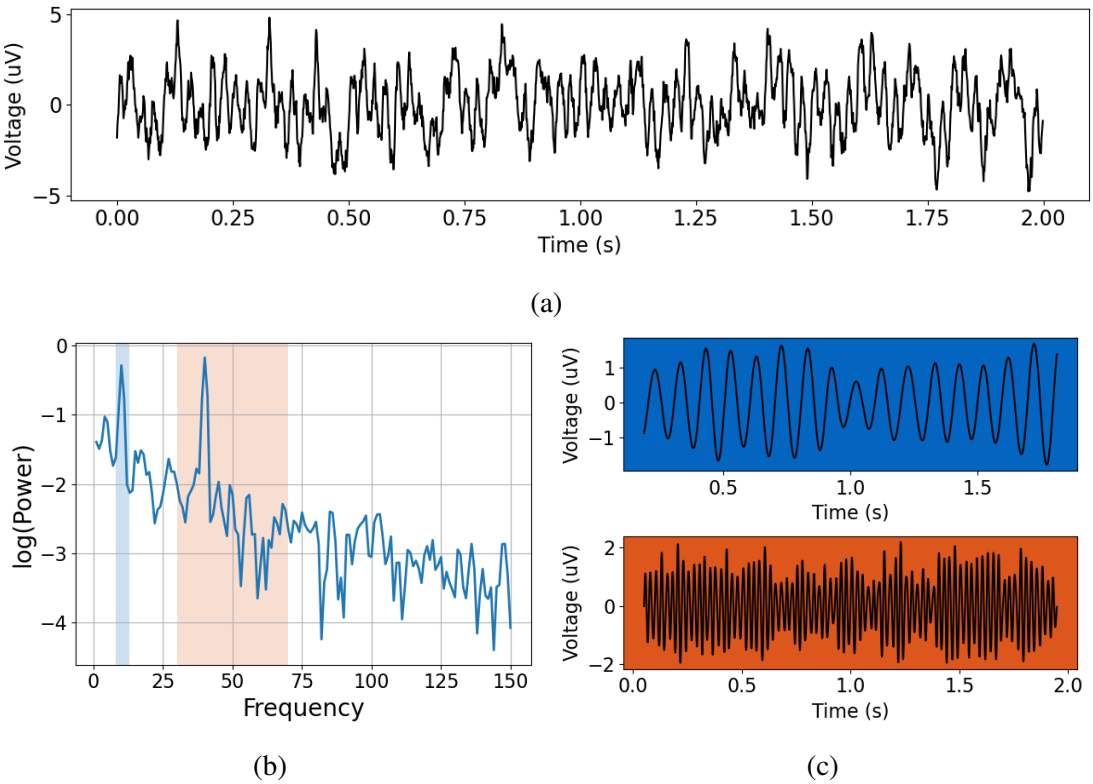

Figure 1. (a) Simulated brain signal composed of: i) simulated synaptic current; ii) sine wave at 10 Hz; iii) sine wave at 40Hz. (b) Simulated signal represented in the frequency domain with color shaded frequency bands: alpha (blue) and gamma (orange). (c) Simulated signal filtered in the alpha (top) and gamma (bottom) bands.

Since oscillatory activity was first observed in brain signals, changes in activity at specific frequencies have been associated to different aspects of animal behavior. For example, activity in the lower bands has been observed to be higher at rest and decrease upon activation of a motor response ([AFS+99], [MLS+07]). The former phenomenon is known as event-related desynchronization (ERD), whereas the latter is known as event-related synchronization (ERS) [Cro98]. Analogously, irregularities of activity at a specific band have been associated to neurological disorders [VK15]. A remarkable observation is that the features of the oscillatory patterns discovered in humans are conserved across other mammals [BLS13]. As shown in Figure 2, the frequency centers vary only slightly across large variation of brain mass.

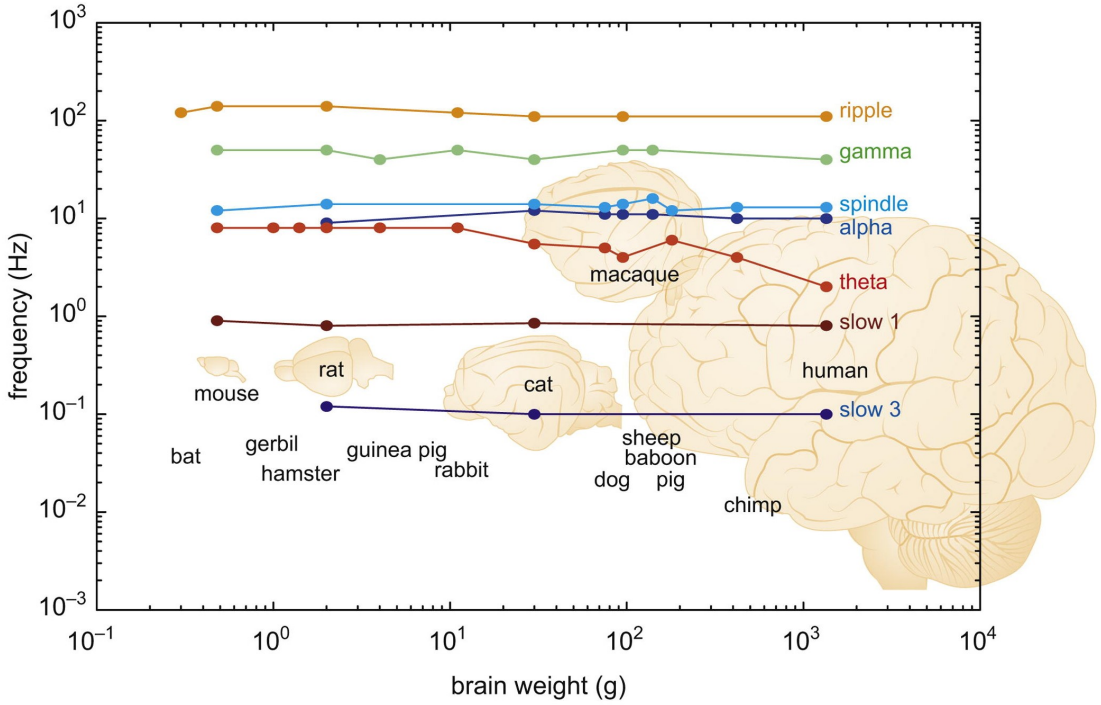

Figure 2. Brain frequencies and their behavioral mappings are preserved across instances of mammalian brain (source [BLS13]).

In more recent decades, research has been focused on the idea that the oscillations are not only the manifestation of specific behavioral phenomena, but that they may be a necessary element that supports the communication between brain regions at different scales ([Fri05], [VKB+15]).

However, interestingly, in the last decades there has been a shift in thinking about the spectral analysis of neural signals. Namely, it has been discovered that not only oscillations are the interesting events. Rather, at higher frequencies (so called "high-gamma") another process is revealed: a change that happens across many frequencies, a

broadband change [Mil10]. Next, we will present evidence that spectral analysis of this high-gamma signal range might not reflect oscillations but rather might be a manifestation of local neuronal firing. Then we will present experimental evidence collected in the last decades which suggests that changes in the higher frequency bands could be a reflection of a broadband change across all frequencies [MSON09].

2.1 Change in high frequency bands reflects local neuronal activity

The idea that local neuronal activity correlates to broadband power changes in the electrical activity measured from the surface of the brain started to take form from experimental evidence in the early 70s [Mil10]. This observation was corroborated later on by the experiment described in [Cro98]. In their work, the authors recorded ECoG signals from subjects who were performing different motor activities. They observed that, during these activities, the spectral power in the gamma and high-gamma bands would increase with respect to the pre-stimulus baseline. It is important to notice that the link between neuronal activity and increase in the gamma band is not direct, as there was no direct recording of the neuronal activity. Rather, they based this conclusion on the fact that the power change was detected in the putative sensorimotor areas.

In a study on 22 human subjects described in [MLS+07], the authors quantify the changes in power in the low (8-32 Hz) and high (76-100 Hz) frequency ranges of ECoG signals. In this study, they confirm that concurrently with motor activity the power in the low range decreases, whereas the power in the high range increases.

Later works began to suggest the idea that high-frequency changes were indicative of broadband changes occurring at each frequency and that changes in the lower frequencies were masked by changes in the lower bands. In other words, the novel emergent concept was that neuronal activity changes were not reflected by changes in a specific frequency (i.e. as an oscillation), but by change across all frequencies.

2.2 High frequency change as evidence of broadband change

The work described in [MZF+09] showed how the broadband changes typically associated to motor movement could hide in reality a broadband change across all frequencies. In their work, the authors recorded ECoG signals from 10 human patients as they performed a motor task. By mapping the cortical area involved in the task to broadband power changes, they demonstrated how this latter can be used as evidence for local neuron activity.

A similar experiment is described in [MSON09]. Twenty epileptic patients performed fixation and hand movements, while ECoG signals were being recorded. The authors were able, after removal of the lower band peaks, to fit a power law to the higher frequencies of the PSD and to show the shift in power during movement (Figure 3).

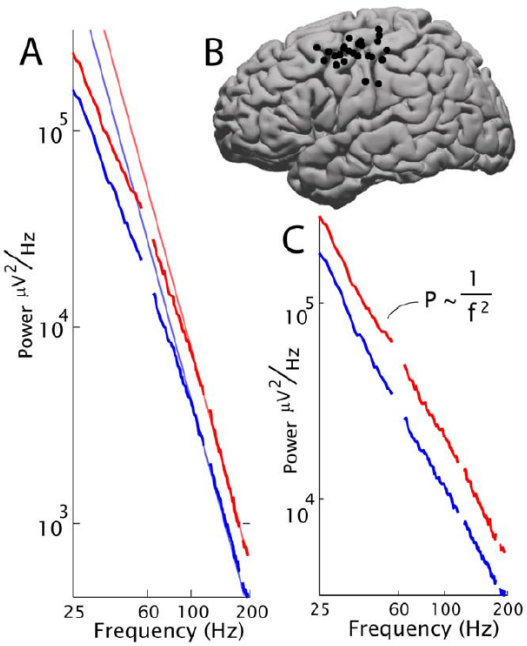

Figure 3. Average PSD from signal recorded at hand motor cortex locations. (A) and (C) show the shift across all frequencies from rest (blue) to movement (red), i.e., a broadband change or a change in aperiodic activity. (B) shows the position of recording electrodes. (source [MSON09])

The experiment described in [MJFK09] further corroborates this idea. In this study, the authors recorded single neuron activity and LFP activity in 20 patients affected by epilepsy. They observed the already known relationship between local neuron firing and change in narrow band oscillations of LFP. More importantly, they proposed that broadband shifts are much more powerful predictors of neuronal activity, compared to narrow band oscillation analysis.

This research has demonstrated the importance of broadband changes. However, what exactly are these broadband signals? This broadband power reflects the presence of all those aperiodic activities that leave their trace in brain recordings and in which the periodic components are embedded [DHP+20]. In brain signals, this aperiodic activity can be characterized as a $1/f^{\chi}$ function, which has decreasing power for increasing frequency values (see Figure 3). This aperiodic component is parametrized by a slope (the exponent in log-log space) and by its shift in power. The concepts of broadband signal and aperiodic component can be considered equivalent. In order to maintain the terminology clear and consistent, we will solely use the term aperiodic component throughout the rest of this work.

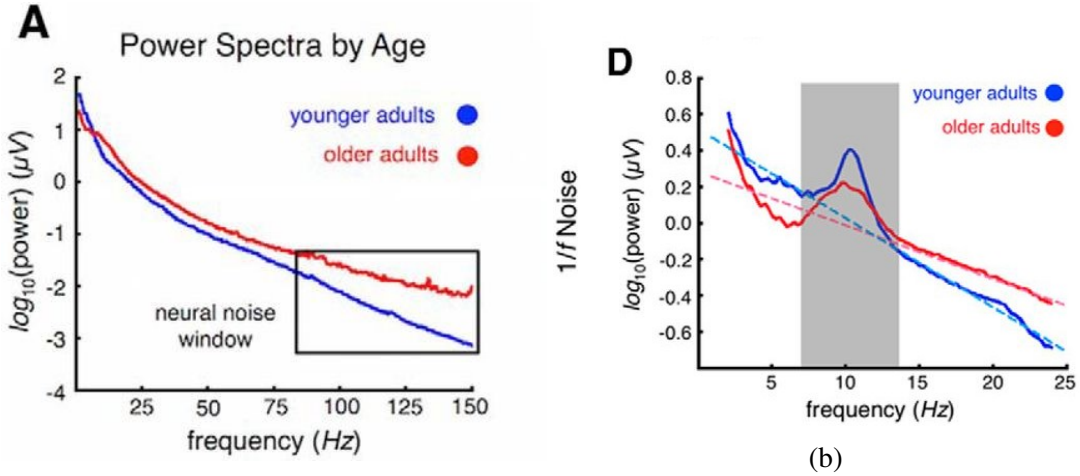

(a) (b)

Figure 4. PSD comparison of younger and older adults. (a) Average PSD of ECoG signals. (b) Average PSD of EEG signals. (source [VKC+15])

2.3 Aperiodic component parameters as physiological biomarkers

The importance of describing the aperiodic component shifts in brain signals goes beyond the ability to predict local neuronal activity. The work described in [RFV+19] shows evidence of a robust relationship between the parameters of the aperiodic component in children with Attention Deficit and Hyperactivity Disorder (ADHD). The authors recorded EEG from ADHD and typically developing children. The PSD was calculated from the EEG and its aperiodic component was extracted. They report that slopes were consistently steeper and the offsets greater in ADHD affected subjects, compared to typically developing subjects.

The work described in [VKC+15] is based on EEG and ECoG data recorded from subjects of different ages. The authors propose that the noise, which in the work is described by the slope of the signal's PSD, increases with age. The plots in Figure 4 show how the $1/f$-shaped PSD is flatter, that is the exponent is closer to zero. This, the authors propose, reflects a noisier, less coordinated neuronal spiking, which in turn is associated with poorer cognitive and motor skills in older adults.

In [GPV17], the authors propose that the slope of the aperiodic component can be used to indicate an imbalance between the levels of synaptic excitation (E) and synaptic inhibition (I). This balance is considered essential for aspects such as neuronal homeostasis, information transmission and working memory maintenance. Building on top of this proposal, the work described in [MVT+20] reports that the aperiodic component calculated from the EEG power spectrum displayed greater steepness in subjects affected by schizophrenia, compared to healthy subjects.

2.4 Motivation

In the last years, evidence that the aperiodic components of a brain's signal spectrum contain relevant information about the brain's processes has been building up. At the same time, more effective tools have appeared and larger amounts of data are made available.

Evidently, there is much more to uncover about these elements of the brain's electrophysiology. With this in mind, we set the goal to explore two specific questions. First, to better understand the neural mechanisms underlying the aperiodic component, we studied the relationship between dendritic calcium spikes and the aperiodic component. Second, we wanted to test whether the aperiodic component could reflect the state of consciousness.

2.4.1 Dendritic calcium spikes and aperiodic component

Dendritic calcium spikes can be generated in apical dendrites of cortical pyramidal cells and have been correlated with animal behavior [XHW+12]. In this work, we use a subset of the data collected in the experiment described in [SL17]. The authors devised a novel method to stimulate dendritic calcium spikes that would avoid the occurrence of confounding factors. By correlating the recording of LFP and surface potentials, the authors demonstrate the possibility of detecting calcium spikes from recorded surface potentials.

In [LBK+20] the authors propose that superficial broadband high gamma activity (BHA) might originate from calcium spikes. In their experiment, the authors recorded field potentials from the auditory and visual cortices of monkeys with laminar multi-electrodes probes. The probe recorded at different cortical depths, while the monkeys underwent auditory and visual stimuli trials. They report two results regarding broadband high gamma activity. For signals recorded at deeper layers, BHA correlated with neuronal activity, whereas neuronal activity could not be accounted for the late BHA in signals recorded closer to the surface. Calcium signaling is largely mediated by N-methyl-D-aspartate (NMDA) receptors. To test the possibility that the late BHA reflects calcium signaling, they performed experiments on one subject to which they administered an NMDA antagonist. They observed that while late-superficial BHA was attenuated with respect to control subjects, the local neuronal activity was not significantly altered.

As the BHA is part of the aperiodic activity, this evidence suggested us the possibility that a relationship between calcium signals and the aperiodic component could be tested and revealed. In order to do that, we went back into the data by [SL17] and directly studied the relationship between the BHA, aperiodic activity and calcium signals.

2.4.2 Conscious experience and aperiodic component

Our second line of investigation revolves around the possibility to link changes in the aperiodic components to changes in state of consciousness.

The experiments described in [SL20] provide evidence that a fundamental mechanism underlying conscious experience is the coupling between distal apical dendrites and the soma of L5 neurons. In this study, mice were injected with three different anesthetics, while recording extracellular activity at different depths in the primary somatosensory cortex (and in the frontal cortex in control experiments). A micro-periscope was used to stimulate the distal apical dendrites. In the awake state, stimulation of the apical dendrites would propagate to the soma. In the unconscious state the propagation was greatly reduced regardless of the anesthetic. Evidence that the anesthetics act on the coupling between the distal dendritic and soma regions comes from the observation that, under anesthesia, the optical stimulation would still affect the stimulated distal dendritic region.

The importance of this coupling mechanism is highlighted in [ASL20]. In this work, pyramidal L5 neurons become the main biological actor supporting conscious processing. As they review the recent experimental evidence in support of this hypothesis, they demonstrate how the low level coupling between the apical dendrites and the basal component of these cell supports the integration of the high level cognitive streams that are believed to be the basis of consciousness. An important part of this idea [SL20, ASL20] is that there are certain receptors (metabotropic glutamate receptors) that control this coupling between the apical and basal compartments.

Here we studied a dataset where electrophysiological recordings were collected from two different brain areas while the animal was in a wakeful resting condition and while the animal was administered a drug that blocks the metabotropic glutamate receptors in the primary sensory cortex (henceforth we will call this condition the "drug" condition). Our question was whether the drug that blocks the coupling between the apical and basal compartments will lead to changes in the aperiodic activity and in the correlation between different cortical areas.

2.5 Contributions

In this work we study the aperiodic component changes of brain electrical activity in two different experimental setups involving mice. In both cases the brain electrical signals are collected with multi-layer arrays of electrodes implanted in the sensorimotor cortex.

In signals recorded during sensory stimulation, we observed an increase of both aperiodic component parameters. The administration of receptor blocking drug in the sensory cortex resulted in a decrease of the aperiodic offset in both primary sensory and motor regions. In this case the correlation between higher and deeper layer within the same region increases in the sensory cortex and decreases in the motor cortex. We also

observed that correlation of the aperiodic component parameters between sensory and motor cortex in the superficial layers dropped, whereas it appeared almost unchanged in deeper layers. Finally, we also observed that spectral connectivity across the layers in the sensory and motor cortex increases after administration of the drug.

3 Methods

3.1 Power Spectral Density

One of the tools used in this work is the Power Spectral Density (PSD). Given a time series, its PSD represents the signal in the frequency domain. When dealing with brain signals, we typically focus on a specific range of frequencies and the PSD gives us the distribution of power in the signal within that range. There are different ways of calculating the PSD of a signal. In this work we use the Welch's method [Wel67] which, according to our experience, is the most widely used in neuroscience studies. In this method, a signal is segmented into fixed sized overlapping windows. Moving away from each window's center, the signal is scaled to zero moving away from the window's center (typically performed by multiplying it by a Hann function). The PSD is then computed by averaging the Fourier transform of each windowed sequence.

In terms of displaying the spectral components of a signal, the same task is accomplished by the Fourier transform. However, calculating the PSD with Welch's method brings two important advantages, compared to the Fourier transform. In fact, averaging the Fourier transform of small segments, can potentially smooth out i) non-stationary components ii) non-systematic noise components. In Figure 5 we compare the FFT and PSD of a simulated signal. The PSD appears smoother and the periodic components are more evident.

3.2 Time-frequency analysis

Extracting the power and phase of a signal with the Fourier transform provides a picture that is a correct representation in the frequency domain of the original signal. Similarly, calculating the PSD of a signal gives a useful representation of its oscillatory components. The picture provided by these methods are based on the assumption that the periodic components of the signal are constant. In other words, they do not provide any information about the time in which these components were present in the signal. In reality, brain recordings, and biological signals in general, are very dynamic in nature. The form of their time series can vary greatly during an experiment, and these changes are typically the very object of a scientific investigation.

Time-frequency analysis is the preferred way to study biological signals, as it overcomes the limitations of Fourier analysis. The tools of time-frequency analysis allow to study and visualize a signal in both its time and frequency domain. Instead of generating the power signature of a signal from its entire duration, it is possible to generate a power signature for each (sampled) point in time.

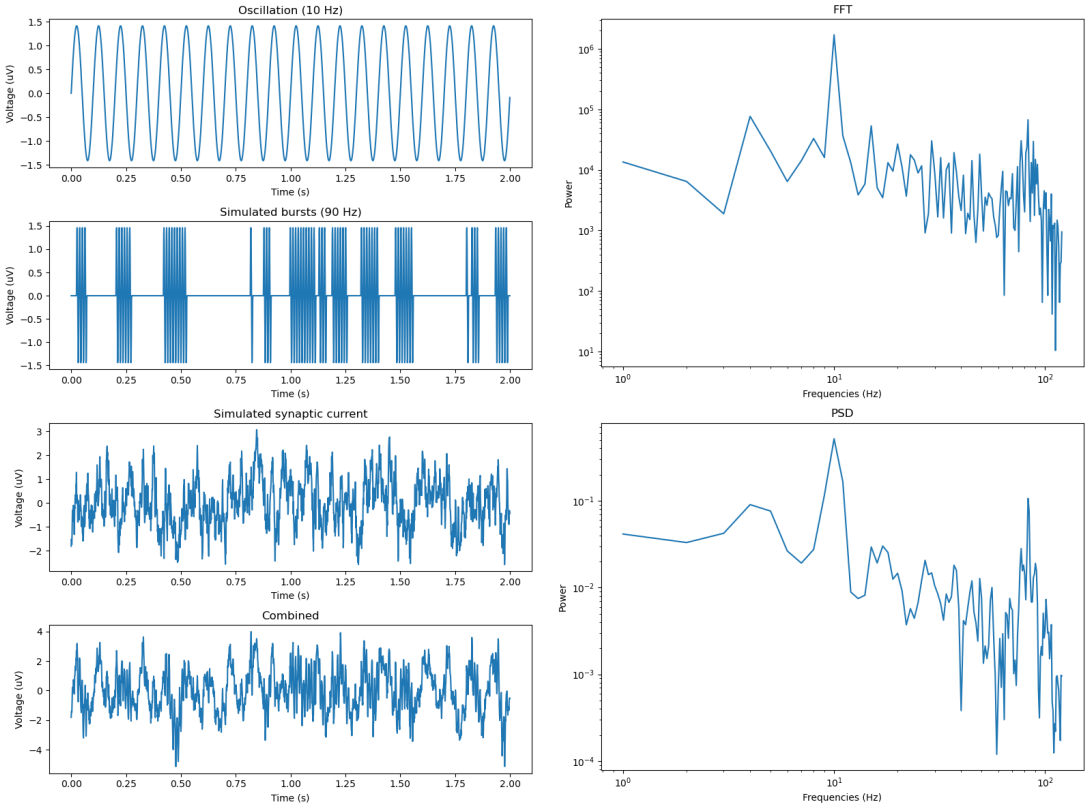

(a) (b)

Figure 5. Comparison between FFT and PSD. (a) Simulated signal (bottom) as a combination of a stationary component at 10 Hz, a non stationary component at 90 Hz and a simulated synaptic current. (b) Fast Fourier Transform (top) and PSD (bottom)

3.2.1 Morlet wavelets

One of the most commonly used methods to perform time-frequency analysis is the convolution of time series with a complex wavelet. In this work we use one specific family of wavelets: the Morlet wavelet.

A Morlet wavelet is defined as the point-wise multiplication of a complex sine wave and a Gaussian. As the complex sine wave is a complex function, the Morlet wavelet is also a complex function. In the following expression we highlight its two components:

$$\psi(t) = \underbrace{e^{i2\pi ft}}_{complex\ sine\ wave} \cdot \underbrace{e^{-0.5(\frac{t}{\sigma})^2}}_{gaussian}$$

In this expression, t is the time variable, i is the imaginary number, f is the frequency,

σ is the width of the window that truncates the Gaussian. The first component in the expression can be expressed through its Eurler's formula, which highlights the real and imaginary parts:

$$e^{i2\pi ft} = cos(2\pi ft) \cdot isin(2\pi ft)$$

Euler's formula two parts can be then separately plotted, as shown in Figure 6a. The second component of the wavelet is the Gaussian, shown in Figure 6b.

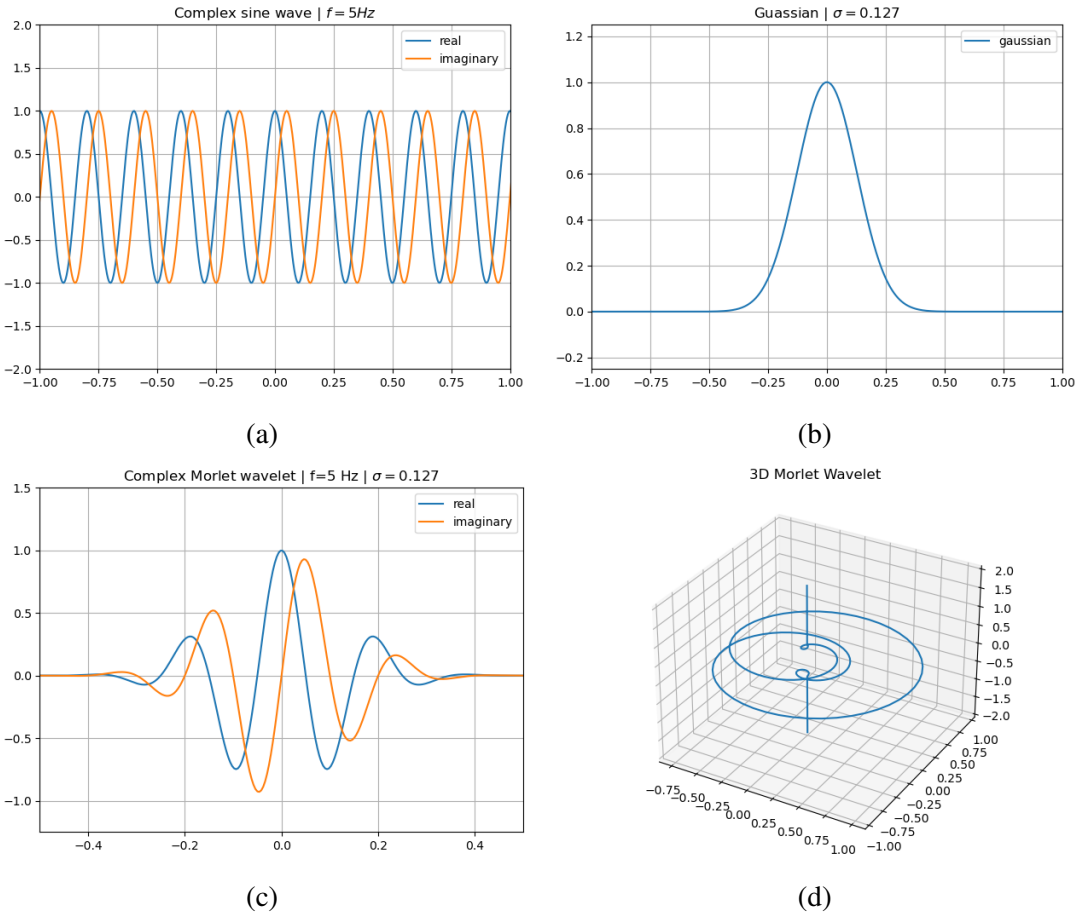

Figure 6. Example of Morlet wavelet. The complex sine wave (a) is multiplied by the Gaussian (b), which has the effect of tapering down to zero the sine cycles (c). (d) 3-dimensional representation of the wavelet.

The multiplication of the complex wave by the Gaussian has the effect of tapering down the complex sine wave as it moves away from the center, as it's shown in Figure 6c. However, since the Morlet wavelet is a complex function, a more appropriate way to

display it is in 3-dimensional space, as we do in Figure 6d. In this representation, we can see the effect of the Gaussian shrinking the cycles moving away from the 0 along the vertical axis.

3.2.2 Morlet wavelet convolution

Applying the Morlet transform to a signal consists in performing a convolution operation between a time series signal and the complex Morlet wavelet. In the convolution, the signal at each time point is dot-product multiplied with the complex Morlet wavelet. The result of this product for each time point is a complex signal from which the power for each frequency and time point can be extracted. An example is given in Figure 7. Figure 7a represents simulated pink noise, in which the power decreases with the increase of frequency. Performing the convolution with the Morlet wavelet at different frequencies results in the power plot in Figure 7b. In this Figure we can see that we have a power value for each time point and frequency point.

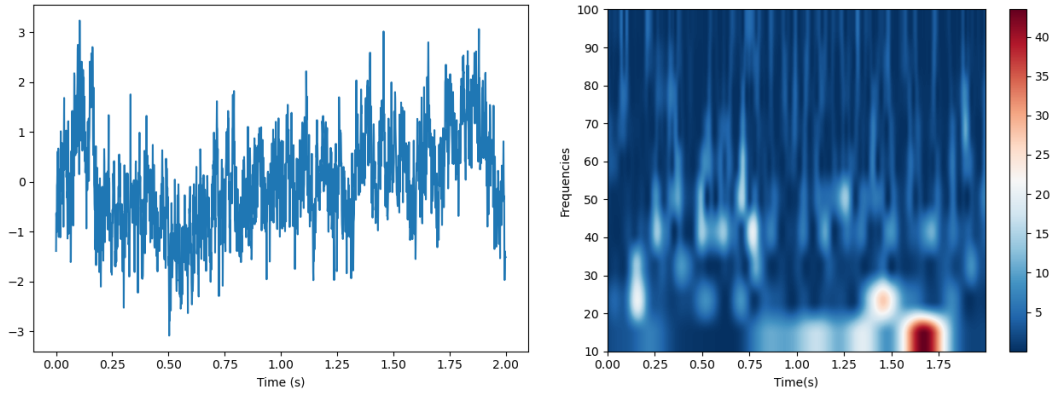

(a) Pink Noise (b) Morlet transform time-frequency power plot

Figure 7. Result of convolution of complex Morlet wavelet with a simulated pink noise signal. The pink noise is created with a simulated power law time series with exponent -1 (a). Morlet wavelets (number of cycles n=7) are convoluted with the simulated signal at 10 different frequencies in the range $\{10 \dots 100\}$.

The standard deviation of the Gaussian can be expressed as:

$$\frac{n}{2\pi f}$$

where n is referred to as the number of cycles, which are the most relevant oscillations of the wavelet. This parameter is particularly important because it regulates the trade-off

between time and frequency precision. An higher number of cycles gives less temporal precision, but more spectral precision.

Using the Morlet wavelet yields three important advantages: i) its lack of sharp edges minimizes the ripple effects ii) the result of the convolution retains the temporal resolution of the time domain signal and iii) it's efficient to compute [Coh19]. In this work we use the Python implementation of the Morlet transformation provided by the MNE library [Gra13].

3.3 Separation of periodic and aperiodic components

Time-Frequency tools like the Morlet transform are useful in localizing changes in power for specific frequency bands. In fact, as mentioned in Section 2, studies of electrophysiology data have greatly focused on analyzing changes in specific frequency bands. However, it is intrinsically difficult to be sure that a particular oscillation is present. Power changes for narrow band frequency might appear as the result of different phenomena. The power might appear to have changed because its center has shifted.

Focusing on narrow band analysis is also complicated by the fact that even signals with no oscillatory components, like white noise or the impulse function, present oscillatory components at each frequency. That is, narrow band changes might appear as a result of changes in other aperiodic components.

The possibility of some of the confounding effects mentioned earlier can be easily shown with simulated data. Let us consider for example the time series generated from a pink noise model in Figure 8.

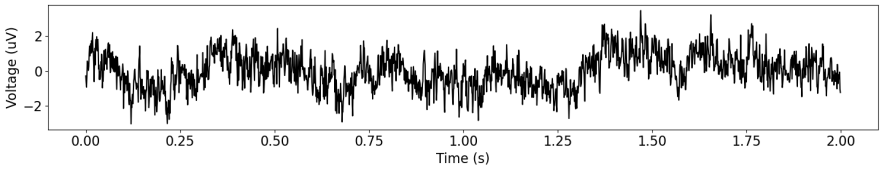

Figure 8. Simulated pink noise: power law with exponent -1 and frequency 1000Hz.

By definition, this time series has no periodic component. However, if we filtered the signal on a specific frequency band, we would find a periodic component that is not there, as shown in Figure 9.

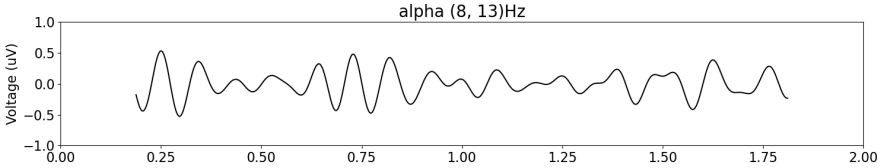

Figure 9. Simulated pink noise: apparent alpha component.

In fact, if we plotted its PSD we will see that the power is present at every frequency (Figure 10).

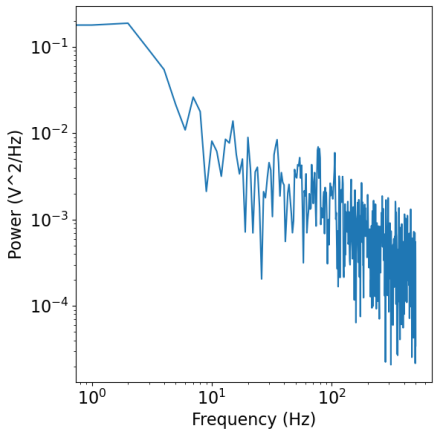

Figure 10. Simulated pink noise: power spectrum.

We have seen how it could be not straightforward to determine the presence of an oscillatory component within a narrow frequency band. There are also other ways in which a change in center or power of an oscillatory component could be just apparent. As discussed in Section 2, neural signals contain, in addition to periodic components, aperiodic activity. This aperiodic activity has a $1/f$ distribution and can be characterized by two parameters: the aperiodic exponent and the aperiodic offset. The aperiodic exponent χ is the exponent in the $1/f^{\chi}$ function. When plotted in the log-log space, it corresponds to the negative slope. The aperiodic offset is the shift of power across frequencies. The offset is probably the most interesting variable, as it is thought to reflect the magnitude of the underlying neural activity: The bigger the offset, the stronger the neural population activity [DHP+20, Mil10]. In Figure 11 we show how a change in one of the aperiodic component parameters can result in an apparent change of a periodic component.

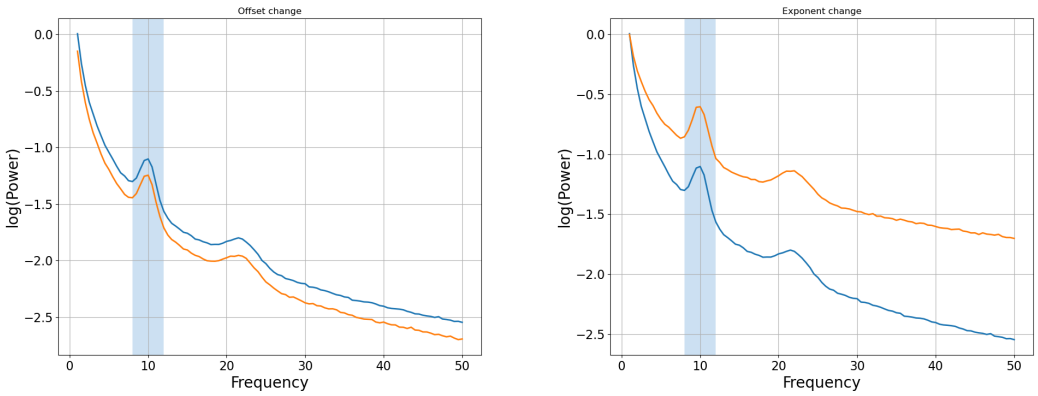

(a) (b)

Figure 11. Apparent change in narrow (8, 12 Hz) band power. (a and b) The blue curve is a simulated PSD with two oscillatory components at 10 and 22 Hz. The aperiodic offset is 0 and aperiodic exponent is 1.5. The range (8,12 Hz) is shaded in blue. (a) The orange curve is the same PSD with aperiodic offset set to -0.15. (b) The orange curve is the same PSD with aperiodic exponent set to 1.

To extract the aperiodic components of brain signals, we employ the analysis tool described in [DHP+20]. Given the PSD computed from a time series, the algorithm allows to separate and extract its periodic and aperiodic components. Of the periodic components, one can extract center frequency, power and bandwidth; of the periodic components, one can extract exponent and offset. The algorithm is implemented in the FOOOF (Fitting Oscillations & One Over F) toolbox written in Python and maintained by one of the authors[1]. In Figure 12 we show the result of applying the FOOOF algorithm to the PSD of the simulated signal shown in Figure 1.

3.4 Spectral Connectivity

The second experimental dataset that we analyze consists of time series recorded simultaneously in the primary sensory and motor cortex. This gave us the opportunity to also study the relationship between change in aperiodic component and the temporal dependence of these two regions. There are several methods to calculate this temporal dependence or connectivity between two signals. We will calculate the spectral coherence connectivity (COH) [AG99], as implemented in the MNE library [Gra13]. COH allows to quantify the level of synchrony between two stationary signals at a specific frequency f [RCV+14].

[1] https://github.com/fooof-tools/fooof

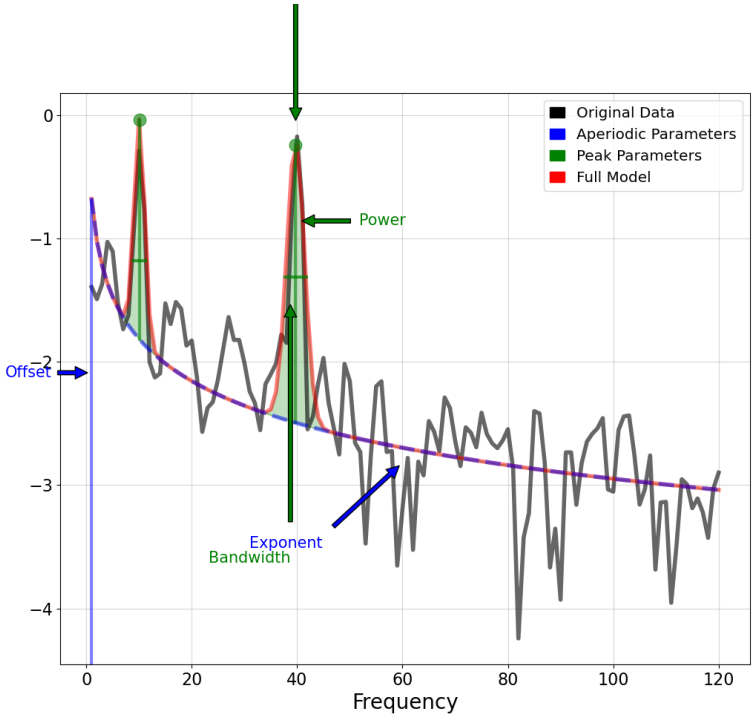

Figure 12. FOOOF model fitting the simulated signal in Figure 1. The algorithm fits a PSD (in red) over the original signal PSD (in black). The original signal contains two periodic components at 10 and 40 Hz, which are highlighted in green. The aperiodic component, parametrized by offset and exponent, is highlighted in blue.

Given the signals coming from channels i and j, the spectral coherence at a frequency f is:

$$COH_{i,j}(f) = \frac{|E[S_{i,j}]|}{\sqrt{E[S_{i,i}] \cdot E[S_{j,j}]}}$$

where E denotes the average of epochs and $S_{i,j}$, $S_{i,j}$ and $S_{i,j}$ are the cross- and auto spectra computed in terms of PSD.

4 Results

We investigated the relationship between physiological changes in the brain and changes in the aperiodic component extracted from recorded brain signals. In this Section we describe the analysis carried out and we comment on the results.

4.1 Sensory evoked dendritic spikes

The first set of data that we used is part of the data collected for the study described in [SL17]. In this work the authors developed a new method to measure calcium dendritic spikes. This method was demonstrated in two different experimental setups. In the first setup dendritic spikes were triggered via optogenetic stimulation. In the second setup, the spikes were triggered through sensory stimulation. In our analysis we used the data collected with the second setup, which is shown in the simplified diagram in Figure 13.

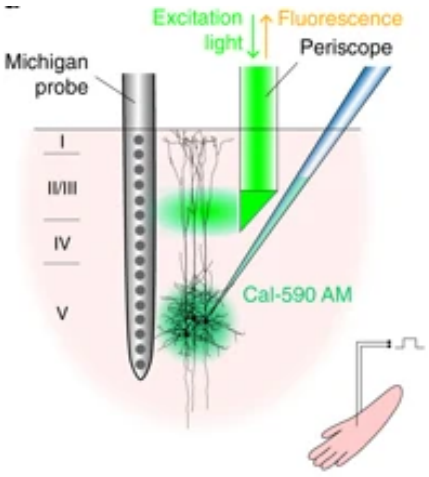

Figure 13. Calcium spikes stimulation and recording setup (source [SL17])

4.1.1 LFP recordings

In this experiment, two different types of data were collected. The first type consists of the recording of extracellular LFP, recorded with a Michigan probe inserted in the hindlimb area of the primary somatosensory cortex in anesthetized rats. The data consists of 16 time series and 50 event timestamps. The 16 time series are the recordings from the 16 electrodes of the Michigan probe across L1 to L5 of the cortex. The timestamp of each event corresponds to the electrical stimulation of the contralateral hindlimb. The 50

events allow to subdivide the data into 50 epochs and correspond to single 1 ms short electrical pulses (100 V) to the contralateral hindpaw.

The original data consists of 16 files, each containing the time-series of an electrode, and a file containing the timestamps of the somatosensory events. In order to analyze the events, we parsed the data using the Python Neo library [SDF+14]. We then used the time series and the events to create MNE objects. Accessing the data with the MNE library gave us in fact the ability to subdivide and access the data by epochs, that is the time windows around each stimulus instant. Figure 14 shows the signals from all 16 electrodes in the first epoch of the dataset.

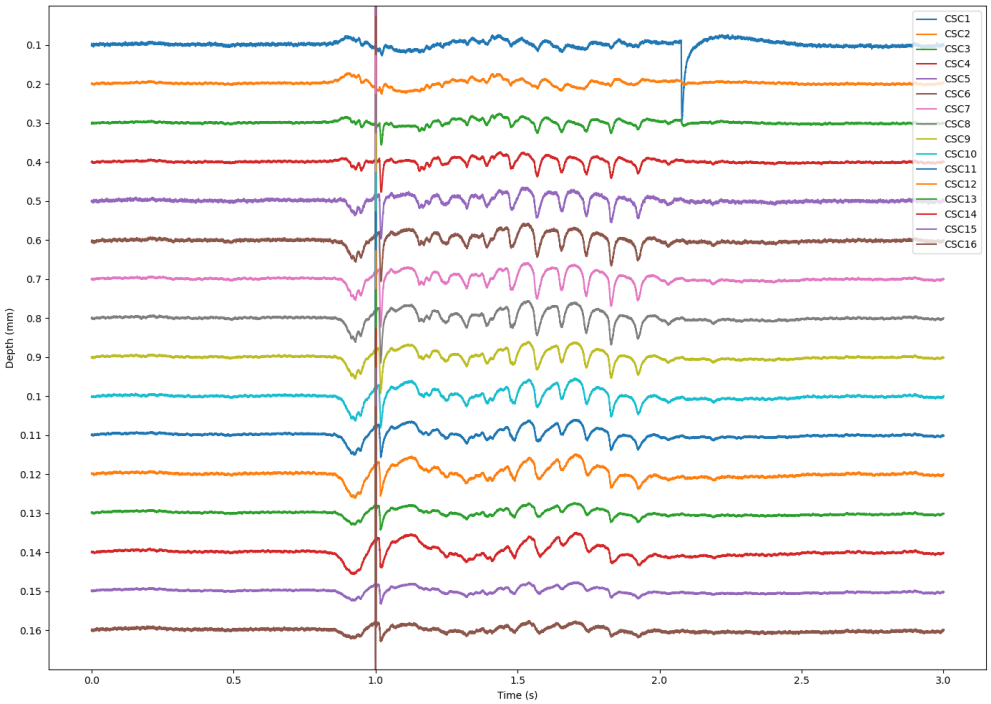

Figure 14. Dendritic LFP time series collected with Michigan probe. The Figure shows the time series of all 16 channels in the first of 50 epochs. On the x-axis we report the time relative to the stimulus event. On the y-axis we indicate the depth from the brain surface of the recording electrode.

Alternatively, it is possible to select a single channel (data from one the probe's electrodes) and analyze it divided into epochs, as shown in Figure 15.

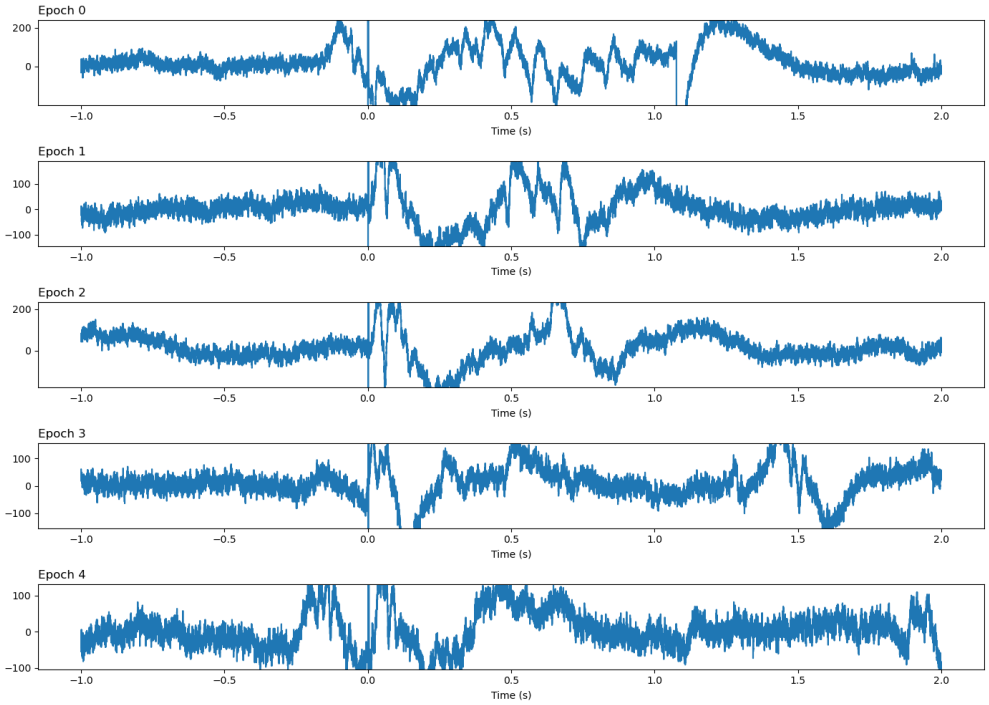

Figure 15. First 5 epochs of data collected by channel CSC1 (top-most electrode).

4.1.2 Fluorescence periscope images

Concurrently with the recording of the extracellular LFP, sequences of fluorescence images in L2/3 were collected. The acquisition setup (see Figure 13) included also a micro-periscope and a high speed CCD camera. During each epoch, the camera recorded a sequence of 80×80 images at a resolution of 125 Hz.

The images are stored using the redshirt format[2] (`.rhd` files), where each epoch is stored in a single file. The images were opened and converted to numpy arrays with the `python-redshirt` library [3]. From each file we extracted the sequences of images in original and normalized form, of which we show examples in Figure 16.

For each image sequence belonging to an epoch we calculate the trace. The trace value of an image consists of the average intensity value of each frame. The average intensity is not calculated out of all the pixels in the image, but only for a pre-calculated subset belonging to the image's region of interest (ROI). Figure 17 shows two examples traces calculated from normalized image sequences.

[2]http://www.redshirtimaging.com/support/dfo.html
[3]https://github.com/jni/python-redshirt

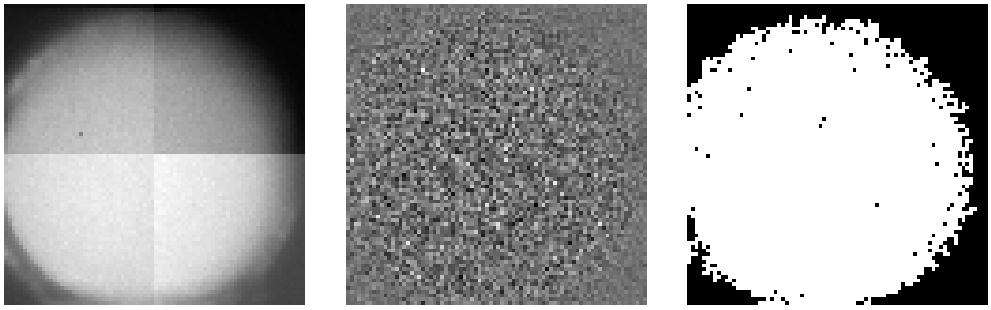

(a) Raw Frame (b) Normalized Frame (c) ROI

Figure 16. Examples of fluorescence images from epoch 5. (a) and (b) show the 5th frame in the epoch. (c) is the ROI calculated for the whole epoch.

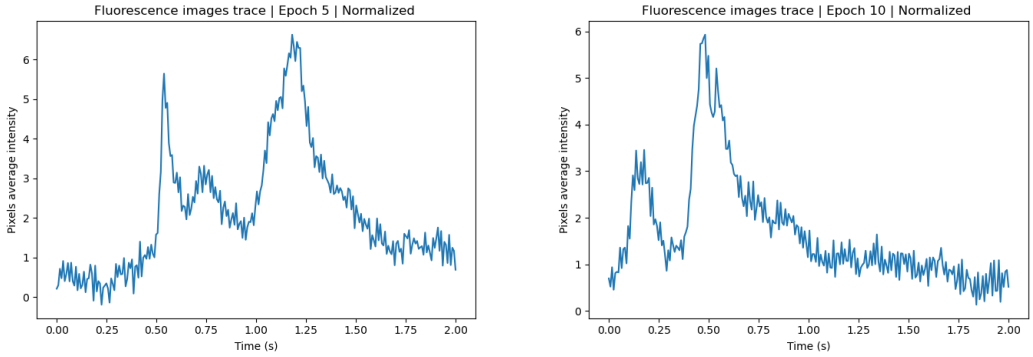

(a) (b)

Figure 17. Examples of fluorescence imaging traces. (a) Epoch 5 (b) Epoch 10.

4.1.3 Time Frequency Analysis

Inspired by the works presented in Section 2, we wanted to investigate what kind of spectral signature changes would be caused by sensory stimulation. We applied the Morlet transform to the LFP time series and inspected the time-frequency power plots before and after the stimulus. We applied the Morlet transform with n=8 cycles on the High Gamma range of frequencies (70-150 Hz) to the evoked response of each channel, where an evoked response is the average of all epochs for a channel. Directly applying the Morlet transform over the whole evoked response did not reveal any visible change in power at high frequencies (Figure 18).

The high power across all frequencies around the stimulus instant offsets the scale of the time-frequency plot. In order to better visualize the frequency components, we used

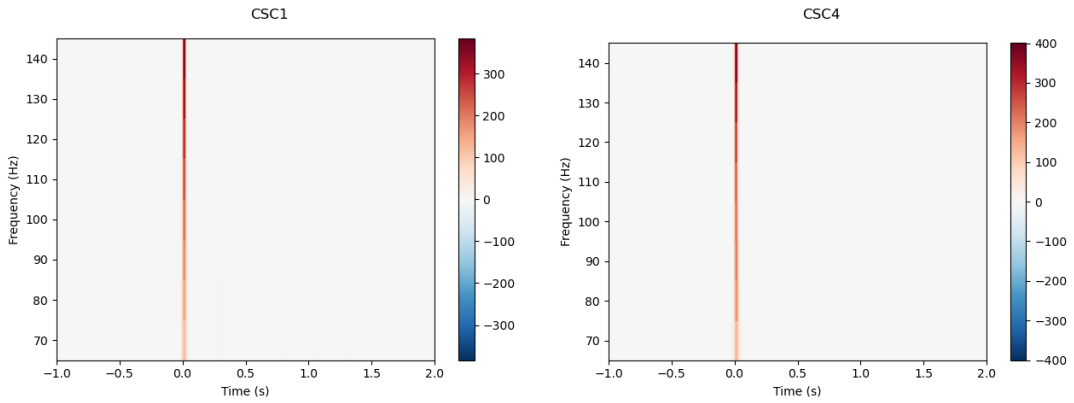

(a) CSC1 (b) CSC4

Figure 18. Morlet Transform applied to the evoked response of channels CSC1 and CSC4.

the following strategy: we applied the Morlet transform and we masked out the signal in a window surrounding the stimulus time. We chose as window the range from -0.2 to 0.2. Furthermore, instead of applying the transform to the evoked response, we applied it to each epoch. Figure 19 shows an example of Morlet transform applied to the same epoch of two different channels. Even in this case we were not able to observe the presence of high frequency components.

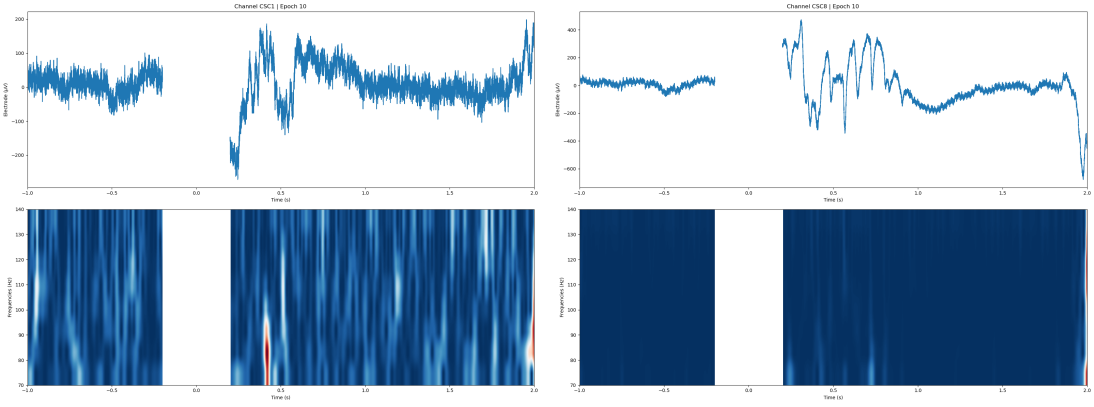

(a) CSC1 (b) CSC8

Figure 19. Morlet Transformation applied to single epochs. At the top of each Figure, the LFP signal is masked around the stimulus instant. At the bottom of each Figure, the Time-Frequency power plot is masked out around the stimulus instant.

4.1.4 Aperiodic component change

We then turned our attention to aperiodic component changes. In particular, our goal was to see whether sensory stimulation would produce consistent changes in the aperiodic components extracted from the signals.

For each epoch, we considered two segments of the signal. The first segment, the *baseline*, is the signal from the beginning of the epoch until 0.2s before the stimulus. The second segment is the signal from 0.2s after the stimulus, until the end of the epoch. We then calculated and plotted the PSD of the two signal segments. We calculated the PSD of each segment using Welch's method and we compared baseline and post-stimulus PSD of each epoch. By visual inspection, we noticed that the post-stimulus PSDs showed an increase in power. Such increase would often reach into the high gamma range of the spectrum. We noticed that this was appearing consistently for each LFP channel and for each epoch. Figure 20 shows two examples of PSD from channels CSC4 and CSC8.

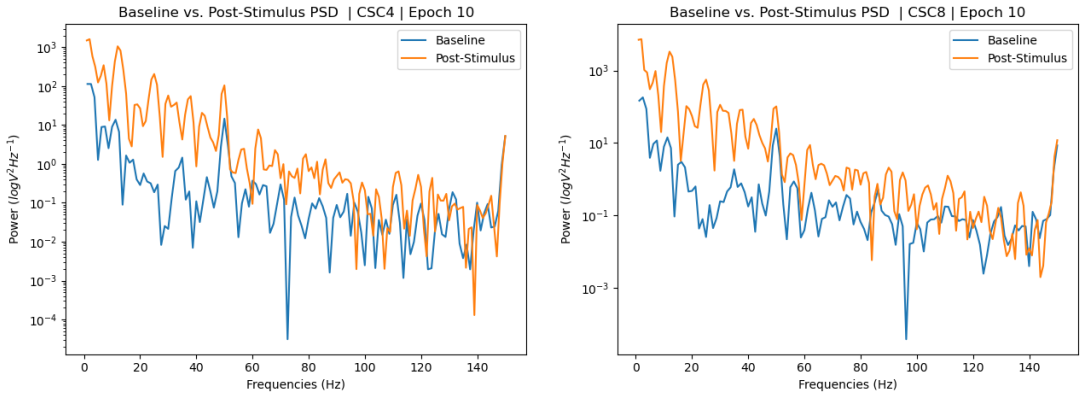

(a) CSC4, epoch 10

(b) CSC8, epoch 10

Figure 20. Comparison of PSD between baseline and post-stimulus signal

In order to quantify this increase in power and test weather this increase is statistically significant, we extracted and compared the aperiodic components of the baseline signal, to the ones of the post-stimulus signal. For each epoch, we used the FOOOF method to extract the offset and exponent of the two epoch segments. The FOOOF model was fitted over the [1, 150] Hz frequency range and using the mode *knee*. In the majority of cases, both offset and exponent appeared to increase after the stimulus. In Figure 21 we compare offset and exponent for all epochs of 2 channels.

To test whether the aperiodic components from baseline and post stimulus are significantly different, we used the Wilcoxon Rank Sum Test. We tested the values of each component computed from the baseline and the post-stimulus segments. We repeated

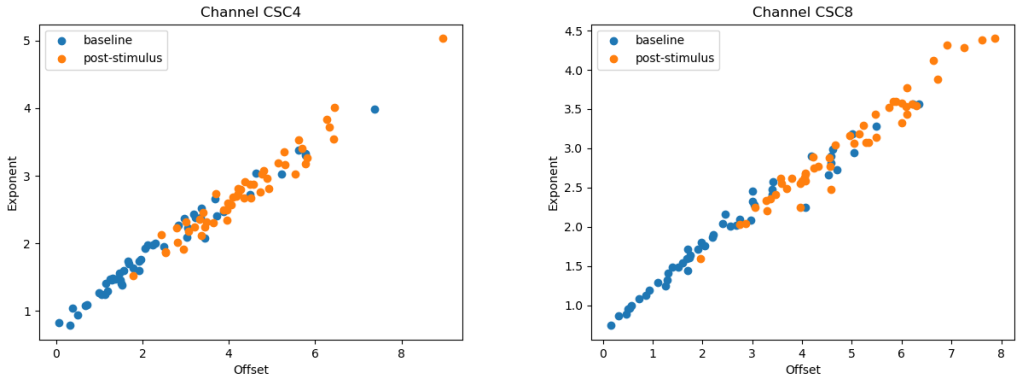

(a) CSC4 (b) CSC8

Figure 21. Comparison of aperiodic parameters between baseline and post-stimulus signal.

this test for channels CSC4 and CSC8. In Table 1 we report the results for channels CSC4 and CSC8.

Channel	offset stat.	offset p-value	exp. stat.	exp. p-value
CSC4	-5.721870	**1.05358e-08**	-5.390967	**7.00795e-08**
CSC8	-6.025199	**1.68902e-09**	-5.976942	**2.27365e-09**

Table 1. Rank Sum Test of aperiodic components computed from baseline vs. computed from post-stimulus epochs of two channels.

From the Table, we can see that the aperiodic components are significantly larger in post-stimulus signals.

4.1.5 Correlation of aperiodic component change with fluorescence intensity

Our next goal was to investigate whether there is a correlation between the aperiodic components in the LFP post-stimulus segments and the intensity of fluorescence.

For each epoch in the fluorescence images data set, we extracted the trace of the frame sequence and calculated its average. We then compared the average of each epoch to both aperiodic component parameters computed on the post-stimulus segments of the LFP data from the same epoch. We repeated this comparison for channels CSC4 and CSC8 (Figure 22).

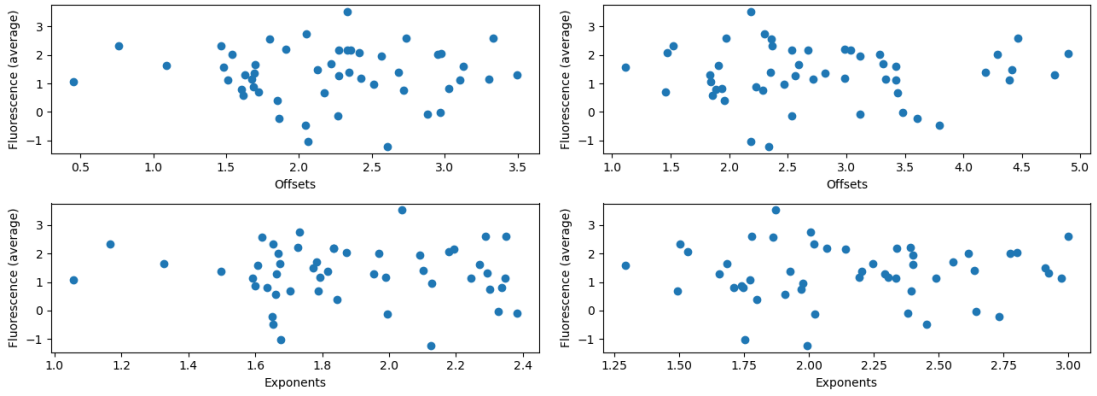

(a) CSC4 (b) CSC8

Figure 22. LFP aperiodic component and fluorescence average trace. Offsets at the top; exponents in the bottom plots.

The scatter plots suggest that there is no correlation between the aperiodic components and the fluorescence intensity. We then calculated the Pearson correlation and show the results in Table 2.

Ch.	Off. corr.	Off. p-value	Exp. corr.	Exp. p-value
CSC4	-0.062185	0.667918	0.087923	0.543742
CSC8	-0.052773	0.715875	0.021753	0.880810

Table 2. Pearson test of aperiodic components and fluorescence average intensity.

4.2 Effect of MCPG on the aperiodic component

In the second part of our work we analyzed the electrophysiologic data of mice who were administered a neuronal receptor blocker in the primary sensory cortex.

4.2.1 Data

As in the previous section, the data used in this analysis was collected in the context of another study performed on mice. In the experimental setup (illustrated in Figure 23), two micro-electrodes arrays were inserted in the primary sensory cortex (S1) and in the primary motor cortex (M1). Each array is made up of 8 electrodes, and each electrode records at 20 kHz. The experiment was performed on three mice and each mouse underwent two recording sessions. In the first session, to which we refer as the *control session*, the probe signals were sampled and recorded for 60 seconds while the mouse was in awake state. In the second session, the *drug* session, the probe signals were recorded for the same duration, but the mouse was administered the metabotropic glutamate receptor blocker (R,S)-α-methyl-4-carboxyphenylglycine (MCPG). The control session of one mouse lasted 45 seconds, instead of 60.

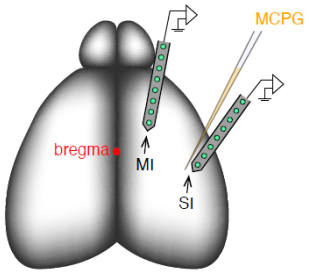

Figure 23. Experimental setup. Two probes record from S1 and M1 in two sessions. In one session the recording occurs during normal wakeful state. In the second session MCPG is administered in S1. (Source Mototaka Suzuki)

The data for each mouse consists of 32 time series: 2 sets of 16 time series (one for the control session and one for the drug session), each set consisting of 8 time series from S1 and 8 time series from M1. The time series were provided in 6 different files (one for the control session and one for the drug session per mouse) encoded in the Intan RHD file format. The data was extracted from the file with the Python Neo library. In Figure 24 we display an example of the data from mouse 1.

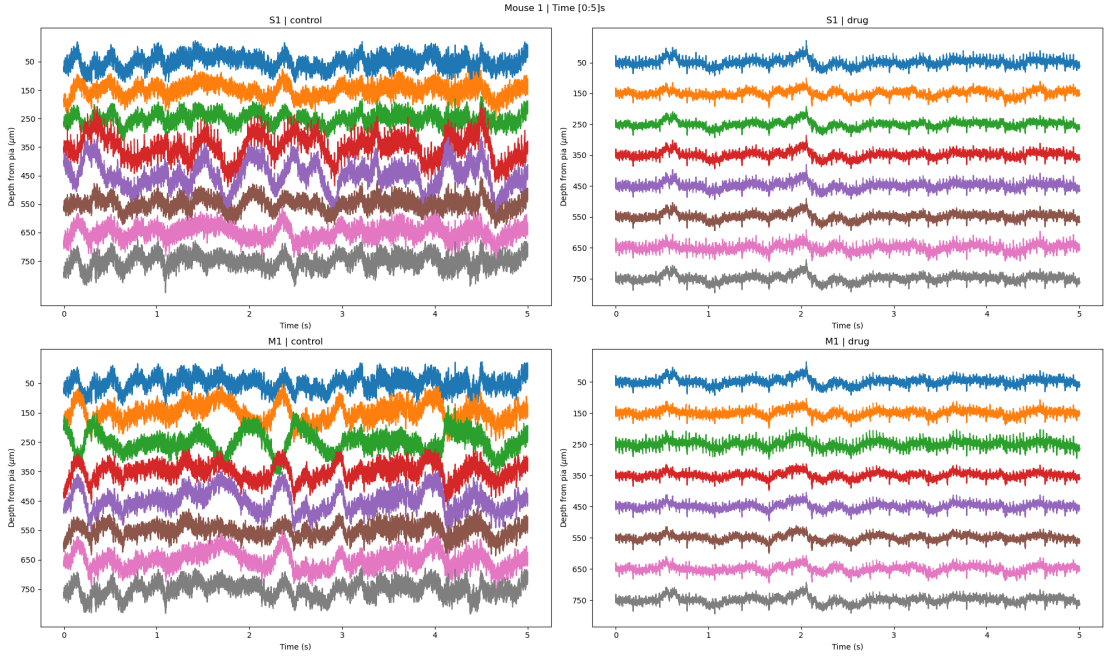

Figure 24. Mouse 1 data extracted from RHD files. Control session data is on the left; drug session data is on the right. S1 data is at the top; M1 data is at the bottom.

4.2.2 Change of aperiodic component

Initially, we computed the PSD of each time series and compare the ones in the control session to the ones in the drug sessions (see Figure 25).

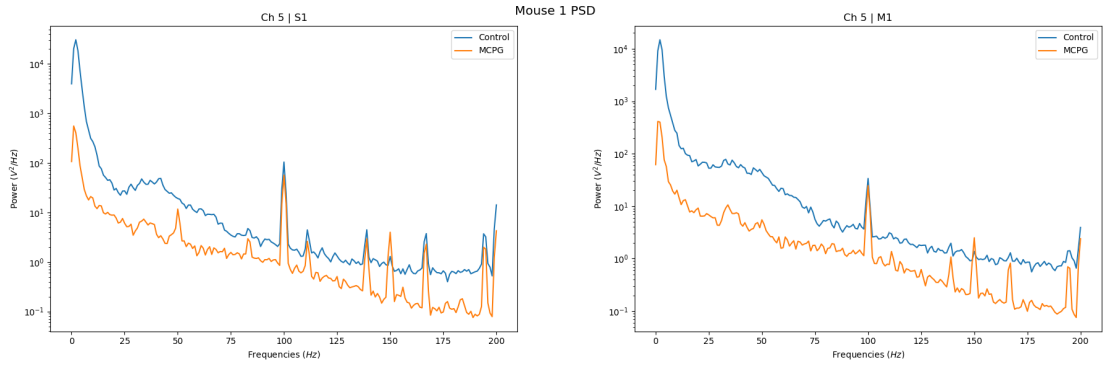

Figure 25. Comparison of Control and MCPG PSD in S1 (left) and M1 (right) from channel 5 of mouse 1.

We computed the PSD using Welch's method (segment length 1 s, overlap length 125 ms, frequency range [0, 200] Hz).

To quantify the effect of the drug on the aperiodic component, we carried out statistical tests on the aperiodic parameters extracted with the FOOOF algorithm. The original data did not include any event information, which would have allowed us to split it into epochs. Therefore, we decided to split the time series of each channel into segments of 5 seconds. We fitted the aperiodic component for each segment and tested the distribution of the aperiodic parameters from channels 3 and 6. In mouse 1 the aperiodic offset of channel 3 in both S1 and M1 was significantly lower (Wilcoxon rank sum test $p < 0.05$) in the drug condition (Table 3).

mouse	region	ch.	off. stats	off. p-value	exp. stats	exp. p-value
1	S1	3	2.203074	**0.027590**	-0.710669	0.477289
1	M1	3	3.482278	**4.9717e-04**	1.208137	0.226994
1	S1	6	1.421338	0.155218	-0.568535	0.569672
1	M1	6	1.563472	0.117942	-0.781736	0.434370

Table 3. Rank-sum statistics of aperiodic components in mouse 1.

In mouse 2 all the aperiodic parameters were significantly lower in the drug condition (Table 4).

mouse	region	ch.	off. stats	off. p-value	exp. stats	exp. p-value
2	S1	3	3.810512	**1.3868e-04**	3.464102	**5.3201e-04**
2	M1	3	3.464102	**5.3201e-04**	3.002221	**0.002680**
2	S1	6	3.925982	**8.6377e-05**	3.464102	**5.3201e-04**
2	M1	6	3.579572	**3.4416e-04**	2.829016	**0.004669**

Table 4. Rank-sum statistics of aperiodic components in mouse 2.

In mouse 3 only the aperiodic offsets in S1 were significantly lower in the drug condition (Table 5).

In Figure 26 we display the aperiodic components calculated from a different channel (5) in S1. The results are similar to the ones of channels 3 and 6.

4.2.3 Correlation of the aperiodic component

In Section 2, we have seen that the effect of the drug in cortical pyramidal neurons is to effectively block the communication between the cell soma and its apical dendrites. As the data consisted of recording at different depths, we decided to investigate how the

mouse	region	ch.	off. stats	off. p-value	exp. stats	exp. p-value
3	S1	3	2.771281	**0.005584**	-0.866025	0.386476
3	M1	3	-0.288675	0.772830	-1.616581	0.105969
3	S1	6	2.309401	**0.020921**	-2.136196	**0.032663**
3	M1	6	0.866025	0.386476	-1.501111	0.133327

Table 5. Rank-sum statistics of aperiodic components in mouse 3.

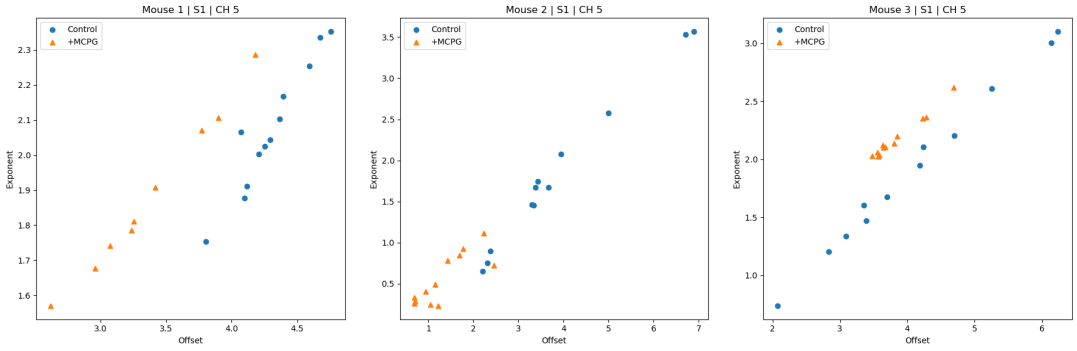

(a) (b) (c)

Figure 26. Comparison of aperiodic parameters extracted from Channel 5 segmented signal recorded in S1 under control and drug conditions. (a) Mouse 1, (b) mouse 2 and (c) mouse 3.

correlation between the aperiodic components would change from the control to the drug condition across regions and channels.

We tested the correlations between channels within a same region. For each condition, we calculated the correlation between the aperiodic components of channels 3 and 6 in S1 and M1. In mouse 1, the correlations of offset and exponent increased within S1 (where the drug was administered), whereas the correlations decreased in M1 (Table 6). In the case of mice 2 and 3, there was a very small reduction in correlation (Tables 7 and 8).

Region	Param.	Control Corr.	Drug Corr.	Corr. Diff.
S1	Offset	0.693767	0.932530	-0.238763
M1	Offset	0.608459	-0.085872	0.694331
S1	Exponent	0.840430	0.927890	-0.087460
M1	Exponent	0.658056	-0.145179	0.803234

Table 6. Same region correlations between channel 3 and 6 of mouse 1.

Region	Param.	Control Corr.	Drug Corr.	Corr. Diff.
S1	Offset	0.986364	0.949583	0.036780
M1	Offset	0.983499	0.966827	0.016672
S1	Exponent	0.991466	0.968321	0.023145
M1	Exponent	0.991062	0.973662	0.017401

Table 7. Same region correlations between channel 3 and 6 of mouse 2.

Region	Param.	Control Corr.	Drug Corr.	Corr. Diff.
S1	Offset	0.900439	0.887913	0.012526
M1	Offset	0.971579	0.919360	0.052219
S1	Exponent	0.941324	0.852169	0.089155
M1	Exponent	0.973505	0.904984	0.068521

Table 8. Same region correlations between channel 3 and 6 of mouse 3.

Our second type of test focused on the correlations between the same channel (that is from the same signal at approximately the same depth) in different regions. We calculated the correlation between the channels 3 of S1 and M1, and the same for channel 6. In mouse 1, the correlation of channel 3 decreased from the control to the drug condition, whereas the correlation of channel 6 did not change (Table 9).

Channel	Param.	Control Corr.	Drug Corr.	Corr. Diff.
3	Offset	0.940566	-0.202960	1.143526
6	Offset	0.530571	0.587566	-0.056996
3	Exponent	0.956948	-0.162534	1.119481
6	Exponent	0.658762	0.598330	0.060432

Table 9. Same channel correlations between S1 and M1 of mouse 1.

In the case of mouse 2 the correlations slightly decreased (Table 10), and also in mouse 3 all correlations decreased (Table 11).

Channel	Param.	Control Corr.	Drug Corr.	Corr. Diff.
3	Offset	0.915902	0.892690	0.023211
6	Offset	0.919616	0.916108	0.003508
3	Exponent	0.961923	0.937991	0.023933
6	Exponent	0.949851	0.943401	0.006450

Table 10. Same channel correlations between S1 and M1 of mouse 2.

Channel	Param.	Control Corr.	Drug Corr.	Corr. Diff.
3	Offset	0.683007	0.231849	0.451159
6	Offset	0.697214	0.069425	0.627789
3	Exponent	0.817048	0.253664	0.563385
6	Exponent	0.828869	0.067379	0.761490

Table 11. Same channel correlations between S1 and M1 of mouse 3.

4.2.4 Cross-region connectivity

We studied how connectivity changes from the control condition to the drug condition. We calculated the connectivity between channel 3 of each region with the MNE[4]

[4]https://mne.tools/stable/generated/mne.connectivity.spectral_connectivity.html

`spectral_connectivity` function (frequency range [1, 150] Hz, method COH). In all mice we found that the connectivity between channel 3 appears greater in the drug condition case, across the whole frequency range (Figure 27, 28 and 29).

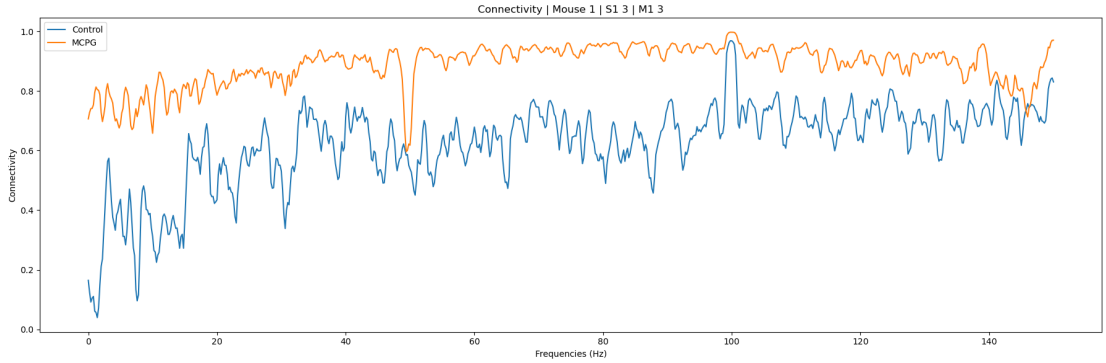

Figure 27. Spectral connectivity between channel 3 in S1 and M1 of mouse 1.

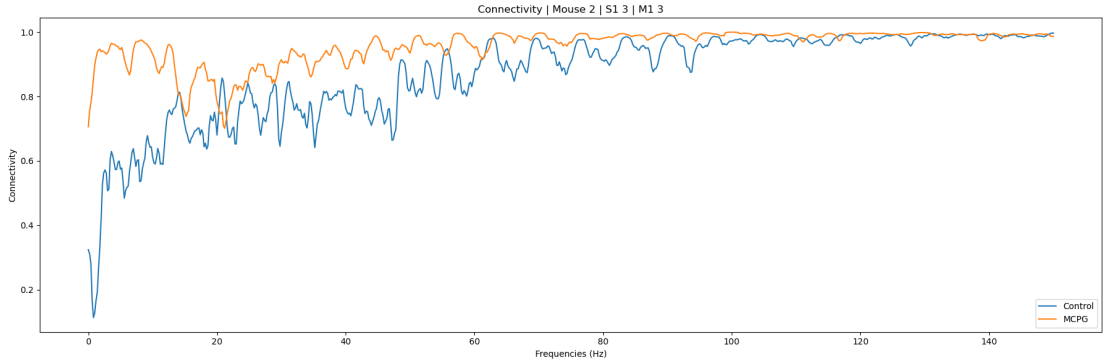

Figure 28. Spectral connectivity between channel 3 in S1 and M1 of mouse 2.

4.2.5 Full connectivity

From the results of the previous section, it appeared as if the difference in connectivity was smallest in the high-gamma range. Since we were expecting a decrease in connectivity, we decided to calculate the connectivity between all channels within that range, as we suspected it would potentially show a decrease in connectivity across other channels. Figure 32 visualizes the 32 highest connectivity values between each pair of channels. By visual inspection, the connectivity appears to increase within the region were the drug was administered and also between S1 and the first layer of M1. Connectivity within M1 increases as well, although by a smaller amount than in S1.

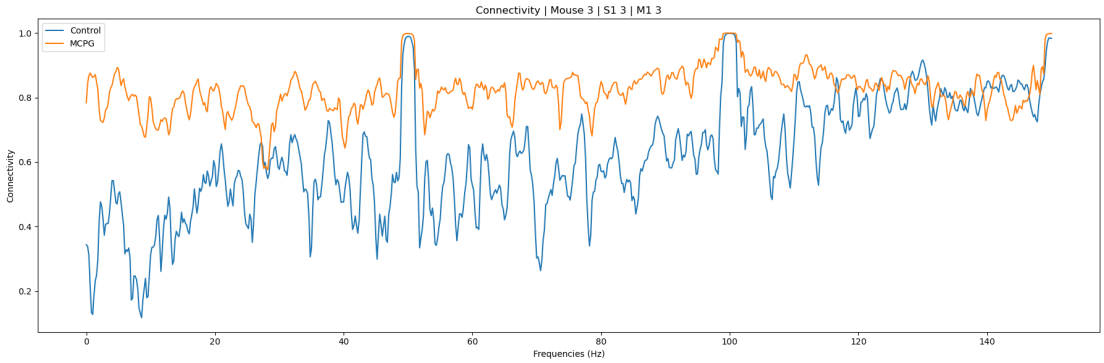

Figure 29. Spectral connectivity between channel 3 in S1 and M1 of mouse 3.

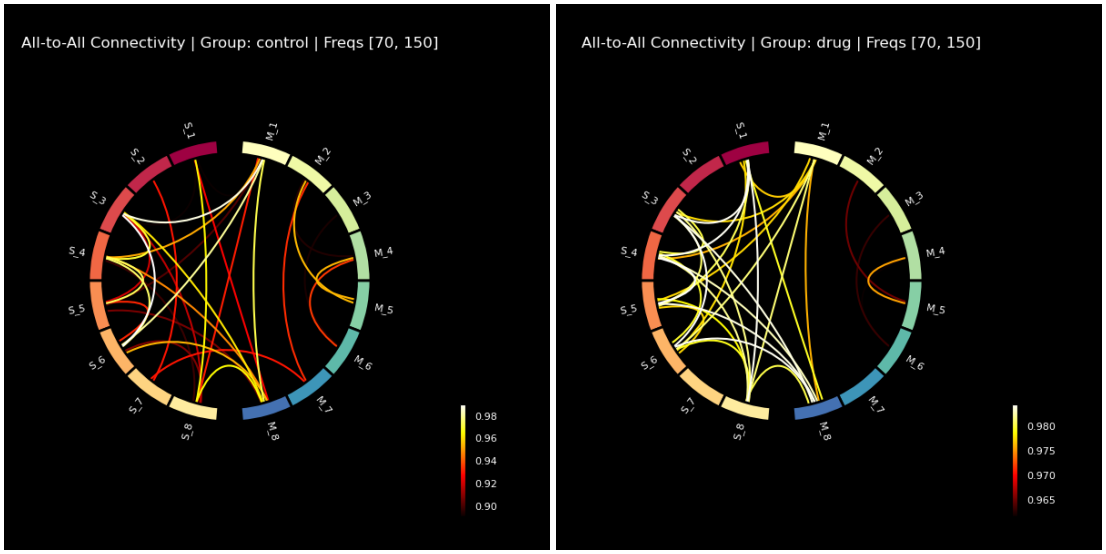

(a) Control (b) Drug

Figure 30. Full connectivity calculated with COH method on mouse 1 data. Left: control condition. Right: drug condition. Only the 32 highest connectivity values are shown.

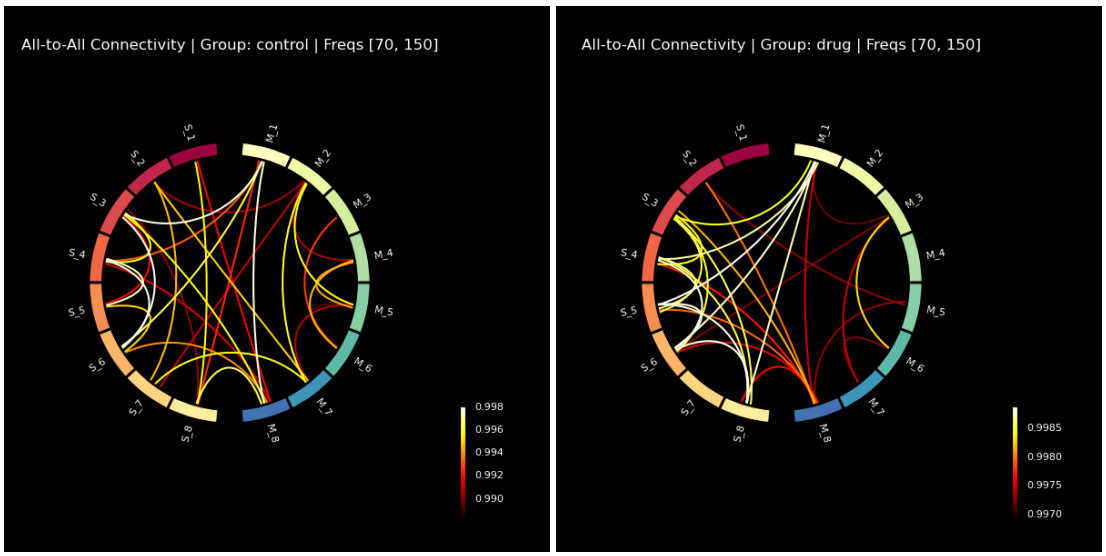

(a) Control (b) Drug

Figure 31. Full connectivity calculated with COH method on mouse 2 data. Left: control condition. Right: drug condition. Only the 32 highest connectivity values are shown.

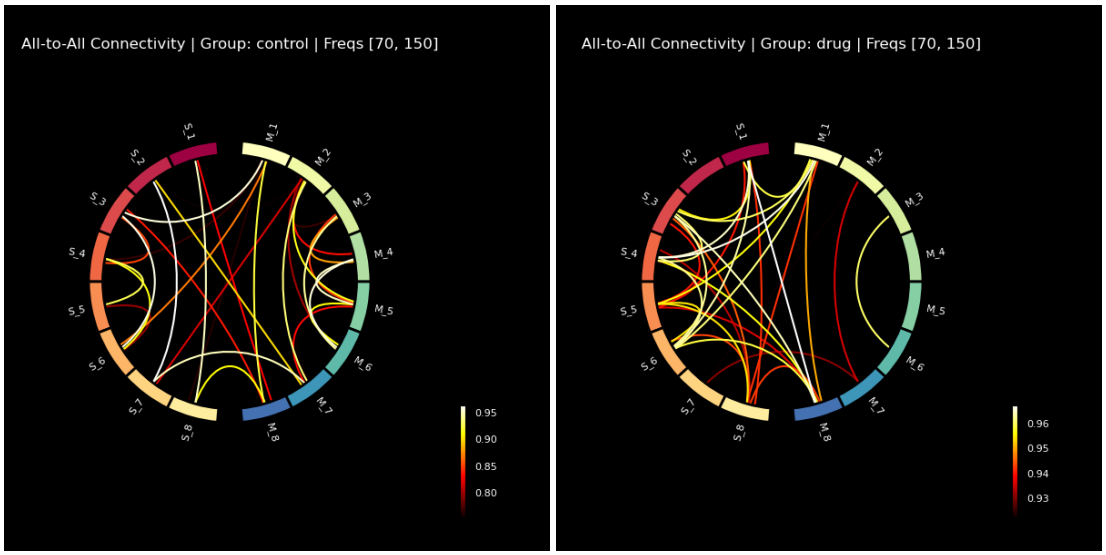

(a) Control (b) Drug

Figure 32. Full connectivity calculated with COH method on mouse 3 data. Left: control condition. Right: drug condition. Only the 32 highest connectivity values are shown.

5 Discussion

In this section, we review our initial motivations in the light of the analysis work carried out, commenting also on the problems encountered and new questions that have arisen.

The general goal of this study was to shine a light on the mechanisms that explain changes in aperiodic component. Our first line of investigation was focused on the relationship between calcium spikes and changes in the aperiodic component parameters. By extracting the aperiodic component parameters, we were able to test the relationship between change in aperiodic component and calcium spikes. This work was motivated by a previous hypothesis by [LBK$^+$20] who suggested that a shift in aperiodic component might be related to dendritic calcium spikes.

The analysis of the relationship between change in aperiodic component and calcium imaging data was inconclusive. We were not able to find any correlation between the calcium intensity values and the aperiodic component. It is worth noting that the calcium imaging dataset had not event data associated to it, therefore we were not able to precisely determine the baseline and post-stimulus segments within a frame sequence. However, as we knew beforehand that calcium signals are more sluggish temporally then we averaged over a longer time window (1.25 s) and hence this problem is not likely to have affected the results. We were able to easily extract image sequences from the calcium imaging dataset and the average intensities that we extracted did indeed suggest the occurrence of a spike (and sometimes two). However, since we were not able to recognize these events through visual inspection and images themselves looked as their four quadrants had different intensities (see Figure 17a), we are left with the suspicion that the algorithm used to read the images from file might not have rendered them correctly.

In the second part of our work we were asking whether changes in aperiodic component could reflect changes in the state of coupling between the apical and basal compartments. This coupling [SL20] as manipulated by the drug MCPG, has been claimed to be crucial for the state of consciousness [ASL20]. The drop in the offset of the aperiodic component was significant in the drug condition for all mice in the primary somatosensory (S1) area. This is somewhat expected: the drug reduces neural firing and as the offset tracks average firing activity in the cortex, the drug should indeed lead to a decrease in the offset. Interestingly, however, in mice 1 and 2 the offset also dropped in the primary motor area (M1). This is somewhat unexpected, as the drug is only applied in the primary somatosensory area. Most likely there is a recurrent loop between S1 and M1, hence uncoupling the neurons in S1 would lead to changes also in M1 [ASL20].

When we studied the change in correlation between signals in different regions, we could not find consistency in the results from the three mice. However, we found the results for mouse 1 quite interesting. In the drug condition, the correlation of the aperiodic component between channels 3 and 6 in the motor cortex dropped, although the drug was administered in the sensory cortex, where the correlation instead increased. A possible interpretation could be the following. The decoupling of distal and somatic

compartment in S1 has shown to cause a reduction in somatic and dendritic response [SL20]. In a state of weak activity, a high correlation in S1 could appear simply because the aperiodic component parameters are low and relatively constant. The decrease in correlation between channel 3 of S1 and M1 could be due to the fact that, the decrease in activity of S1 resulted in a disruption of the input of M1 at the level of the distal compartment. Such disruption could in turn explain the decreased correlation between channel 3 and 6 in M1. Unfortunately, this interesting pattern was not observed for the two other mice. At least visually, the difference (from control to drug condition) in signal dynamics that we see in the data from mouse 1 (Figure 24) are very different in mouse 2 (Figure 33) and 3 (Figure 34).

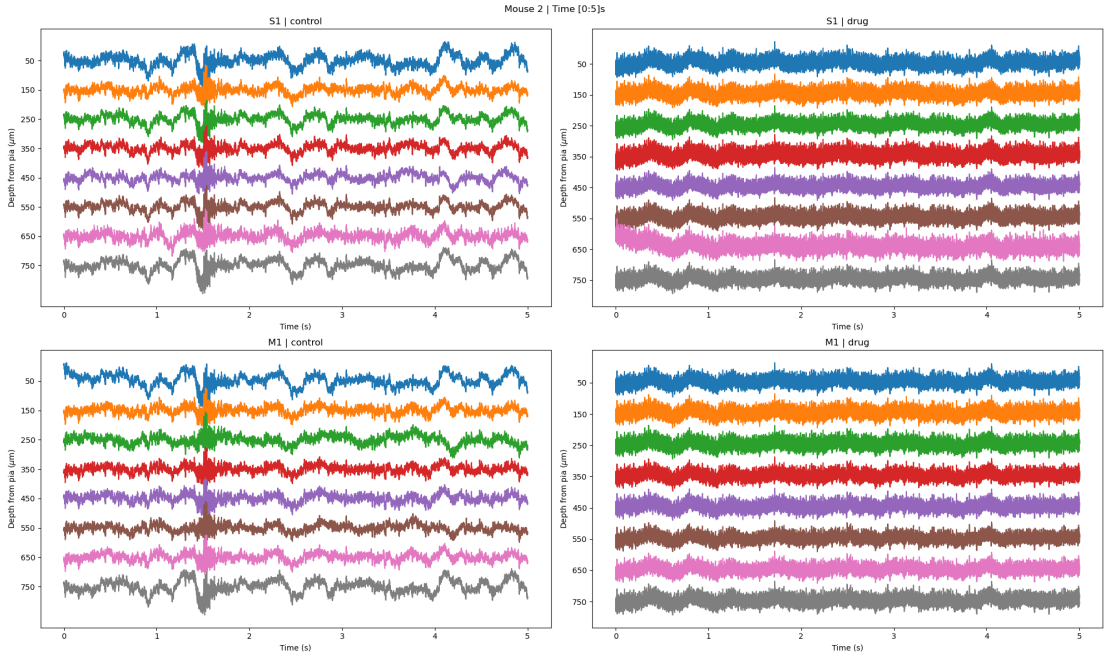

Figure 33. Mouse 2 data extracted from RHD files.

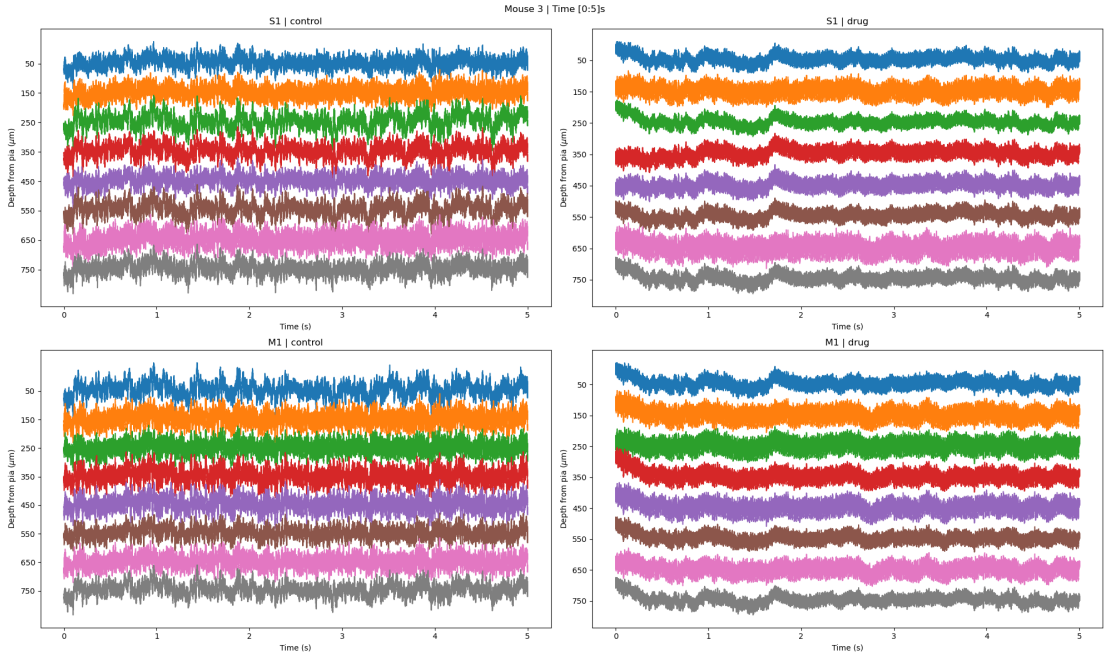

Figure 34. Mouse 3 data extracted from RHD files.

6 Conclusion

In this work we analyzed electrophysiology and fluorescence data recorded in two different experimental setups and explored the relationships between physiological changes in the recorded areas and changes in the aperiodic component parameters. Our analysis was mainly based on the FOOOF algorithm, which allows to separate periodic and aperiodic components in brain recordings. We also used Morlet wavelet transform to study the temporal dynamics of the power spectrum and we used spectral coherence connectivity to study the relationship between aperiodic component changes and functional connectivity.

First, we analyzed the relationship between calcium spikes and the aperiodic component. We observed that, after sensory stimulation, aperiodic offset and exponent in channels CSC4 and CS8 significantly increased. However, there was no correlation between the calcium signals and the aperiodic component. Hence, our results do not support the idea that calcium spikes underlie aperiodic signals in the cortex.

Secondly, we analyzed how the administration of metabotropic receptor blocker in the primary sensory cortex (S1) affected the aperiodic component. In two out of three mice, the administration of neuronal receptor blocker drug MCPG correlated with a decrease of both aperiodic offset and exponent. We then explored the correlation of aperiodic components across different layers and regions. Under the drug condition, correlation within S1 increased, whereas it decreased in the primary motor cortex (M1) in one mouse out of three. In the same mouse, we found that correlation in a higher layer increased, whereas it decreased in a deeper layer.

Finally, we also studied the change in functional connectivity under the drug condition. We found that in one mouse the spectral coherence calculated in the high gamma frequency range increased in S1, between the first and last channels of S1 and M1 and, by a smaller amount in M1.

As this study progressed, we realized that there are a few ways in which we would like this work to be extended and improved upon. Since calcium spikes occur at a known location, we think that a possible development would be the study of the temporal dynamics of the aperiodic component. Does it change in the same way across the layers and over the post-stimulus time frame? For example, from the work described in [LBK$^+$20], we should expect an aperiodic offset change to happen later in the higher layers.

Another possible line of investigation is offered by the calcium imaging dataset that we analyzed in the first part of our study. We were not able to find a correlation between the aperiodic component and the average intensity of the fluorescence images. We could first investigate whether there are other decoders available to read and pre-process the fluorescence images, in order to produce more truthful frames. Secondly, instead of using the simple average intensity, we could calculate different features. For example,

we could estimate a baseline and compute the max difference in intensity with respect to the baseline.

Finally, we would like to explore the relationship between functional connectivity and the change in aperiodic component. For example, we could investigate a relationship between the change in correlation between two channels from control to drug condition, and the change in connectivity. It has been proposed that a decrease in aperiodic exponent reflects an increase in noise and poorer synchronization ([RFV+19], [VKC+15]). This suggests that we could study if there is a relationship between the aperiodic exponent and a decrease in connectivity.

Taken together, this work analysed novel data from the mouse cortex, applied some recently developed tools on these data and made several preliminary observations that will be useful for a better characterization of the neural dynamics in health and disease.

References

[AFS+99] F. Aoki, E.E. Fetz, L. Shupe, E. Lettich, and G.A. Ojemann. Increased gamma-range activity in human sensorimotor cortex during performance of visuomotor tasks. *Clinical Neurophysiology*, 110(3):524–537, Mar 1999.

[AG99] Frank G. Andres and Christian Gerloff. Coherence of sequential movements and motor learning:. *Journal of Clinical Neurophysiology*, 16(6):520, Nov 1999.

[ASL20] Jaan Aru, Mototaka Suzuki, and Matthew E. Larkum. Cellular mechanisms of conscious processing. *Trends in Cognitive Sciences*, 24(10):814–825, Oct 2020.

[Ber29] Hans Berger. Über das elektrenkephalogramm des menschen. *Archiv für Psychiatrie und Nervenkrankheiten*, 87(1):527–570, Dec 1929.

[BLS13] György Buzsáki, Nikos Logothetis, and Wolf Singer. Scaling brain size, keeping timing: Evolutionary preservation of brain rhythms. *Neuron*, 80(3):751–764, Oct 2013.

[Buz04] G. Buzsaki. Neuronal oscillations in cortical networks. *Science*, 304(5679):1926–1929, Jun 2004.

[Coh19] Michael X. Cohen. A better way to define and describe morlet wavelets for time-frequency analysis. *NeuroImage*, 199:81–86, 10 2019.

[Cro98] N. Crone. Functional mapping of human sensorimotor cortex with electrocorticographic spectral analysis. ii. event-related synchronization in the gamma band. *Brain*, 121(12):2301–2315, Dec 1998.

[CS15] Matt Carter and Jennifer Shieh, editors. *Introduction*, pages xxiii–xxviii. Academic Press, San Diego, second edition edition, 2015.

[DHP+20] Thomas Donoghue, Matar Haller, Erik J. Peterson, Paroma Varma, Priyadarshini Sebastian, Richard Gao, Torben Noto, Antonio H. Lara, Joni D. Wallis, Robert T. Knight, Avgusta Shestyuk, and Bradley Voytek. Parameterizing neural power spectra into periodic and aperiodic components. *Nature Neuroscience*, 23:1655–1665, 12 2020.

[Fri05] Pascal Fries. A mechanism for cognitive dynamics: neuronal communication through neuronal coherence. *Trends in Cognitive Sciences*, 9(10):474–480, Oct 2005.

[GK12] Christine Grienberger and Arthur Konnerth. Imaging calcium in neurons. *Neuron*, 73(5):862–885, Mar 2012.

[GPV17] Richard Gao, Erik J. Peterson, and Bradley Voytek. Inferring synaptic excitation/inhibition balance from field potentials. *NeuroImage*, 158:70–78, Sep 2017.

[Gra13] Alexandre Gramfort. Meg and eeg data analysis with mne-python. *Frontiers in Neuroscience*, 7, 2013.

[KNB+09] Steffen Katzner, Ian Nauhaus, Andrea Benucci, Vincent Bonin, Dario L. Ringach, and Matteo Carandini. Local origin of field potentials in visual cortex. *Neuron*, 61:35–41, 1 2009.

[Kre07] Gabriel Kreiman. Brain science: From the very small to the very large. *Current Biology*, 17(17):R768–R770, 2007.

[LBK+20] Marcin Leszczyński, Annamaria Barczak, Yoshinao Kajikawa, Istvan Ulbert, Arnaud Y. Falchier, Idan Tal, Saskia Haegens, Lucia Melloni, Robert T. Knight, and Charles E. Schroeder. Dissociation of broadband high-frequency activity and neuronal firing in the neocortex. *Science Advances*, 6:977–989, 8 2020.

[Mil10] K. J. Miller. Broadband spectral change: Evidence for a macroscale correlate of population firing rate? *Journal of Neuroscience*, 30(19):6477–6479, May 2010.

[MJFK09] Jeremy R. Manning, Joshua Jacobs, Itzhak Fried, and Michael J. Kahana. Broadband shifts in local field potential power spectra are correlated with single-neuron spiking in humans. *Journal of Neuroscience*, 29:13613–13620, 10 2009.

[MLS+07] Kai J. Miller, Eric C. Leuthardt, Gerwin Schalk, Rajesh P.N. Rao, Nicholas R. Anderson, Daniel W. Moran, John W. Miller, and Jeffrey G. Ojemann. Spectral changes in cortical surface potentials during motor movement. *Journal of Neuroscience*, 27:2424–2432, 2 2007.

[MSON09] Kai J. Miller, Larry B. Sorensen, Jeffrey G. Ojemann, and Marcel Den Nijs. Power-law scaling in the brain surface electric potential. *PLoS Computational Biology*, 5, 12 2009.

[MVT+20] Juan L. Molina, Bradley Voytek, Michael L. Thomas, Yash B. Joshi, Savita G. Bhakta, Jo A. Talledo, Neal R. Swerdlow, and Gregory A. Light.

Memantine effects on electroencephalographic measures of putative excitatory/inhibitory balance in schizophrenia. *Biological Psychiatry: Cognitive Neuroscience and Neuroimaging*, 5(6):562–568, Jun 2020.

[MZF+09] K. J. Miller, S. Zanos, E. E. Fetz, M. Den Nijs, and J. G. Ojemann. Decoupling the cortical power spectrum reveals real-time representation of individual finger movements in humans. *Journal of Neuroscience*, 29:3132–3137, 3 2009.

[RCV+14] D. La Rocca, P. Campisi, B. Vegso, P. Cserti, G. Kozmann, F. Babiloni, and F. De Vico Fallani. Human brain distinctiveness based on eeg spectral coherence connectivity. *IEEE Transactions on Biomedical Engineering*, 61(9):2406–2412, Sep 2014.

[RFV+19] Madeline M. Robertson, Sarah Furlong, Bradley Voytek, Thomas Donoghue, Charlotte A. Boettiger, and Margaret A. Sheridan. Eeg power spectral slope differs by adhd status and stimulant medication exposure in early childhood. *Journal of Neurophysiology*, 122(6):2427–2437, Dec 2019.

[SDF+14] Garcia S., Guarino D., Jaillet F., Jennings T.R., Pröpper R., Rautenberg P.L., Rodgers C., Sobolev A., Wachtler T., Yger P., and Davison A.P. Neo: an object model for handling electrophysiology data in multiple formats. *Frontiers in Neuroinformatics*, 8:10, February 2014.

[SL17] Mototaka Suzuki and Matthew E. Larkum. Dendritic calcium spikes are clearly detectable at the cortical surface. *Nature Communications*, 8:1–11, 12 2017.

[SL20] Mototaka Suzuki and Matthew E. Larkum. General anesthesia decouples cortical pyramidal neurons. *Cell*, 180(4):666–676.e13, Feb 2020.

[VK15] Bradley Voytek and Robert T. Knight. Dynamic network communication as a unifying neural basis for cognition, development, aging, and disease. *Biological Psychiatry*, 77(12):1089–1097, Jun 2015.

[VKB+15] Bradley Voytek, Andrew S Kayser, David Badre, David Fegen, Edward F Chang, Nathan E Crone, Josef Parvizi, Robert T Knight, and Mark D'Esposito. Oscillatory dynamics coordinating human frontal networks in support of goal maintenance. *Nature Neuroscience*, 18(9):1318–1324, Sep 2015.

[VKC+15] B. Voytek, M. A. Kramer, J. Case, K. Q. Lepage, Z. R. Tempesta, R. T. Knight, and A. Gazzaley. Age-related changes in 1/f neural electrophysiological noise. *Journal of Neuroscience*, 35(38):13257–13265, Sep 2015.

[Wel67] P. Welch. The use of fast fourier transform for the estimation of power spectra: A method based on time averaging over short, modified periodograms. *IEEE Transactions on Audio and Electroacoustics*, 15(2):70–73, Jun 1967.

[XHW+12] Ning-long Xu, Mark T. Harnett, Stephen R. Williams, Daniel Huber, Daniel H. O'Connor, Karel Svoboda, and Jeffrey C. Magee. Nonlinear dendritic integration of sensory and motor input during an active sensing task. *Nature*, 492(7428):247–251, Dec 2012.

Appendix

I. Glossary

BHA: Broadband high gamma activity
BOLD: BloodOxygen Level Dependent
EEG: Electroencephalography
ECoG: Electrocorticography
ERD: Event-related desynchronization
ERS: Event-related synchronization
FFT: Fast Fourier Transform
LFP: Local field potential
NMDA: N-methyl-D-aspartate
PSD: Power Spectral Density

II. Access to code

The code to produce the presented results, as well as this manuscript, is available (upon request as collaborator) at:

`https://github.com/alessandrostranieri/master_thesis`

III. Licence

Non-exclusive licence to reproduce thesis and make thesis public

I, **Alessandro Stranieri**,

1. herewith grant the University of Tartu a free permit (non-exclusive licence) to

   reproduce, for the purpose of preservation, including for adding to the DSpace digital archives until the expiry of the term of copyright,

   Analysis of the aperiodic component in the mouse neocortex,

   supervised by Jaan Aru.

2. I grant the University of Tartu a permit to make the work specified in p. 1 available to the public via the web environment of the University of Tartu, including via the DSpace digital archives, under the Creative Commons licence CC BY NC ND 3.0, which allows, by giving appropriate credit to the author, to reproduce, distribute the work and communicate it to the public, and prohibits the creation of derivative works and any commercial use of the work until the expiry of the term of copyright.

3. I am aware of the fact that the author retains the rights specified in p. 1 and 2.

4. I certify that granting the non-exclusive licence does not infringe other persons' intellectual property rights or rights arising from the personal data protection legislation.

Alessandro Stranieri
14/05/2021